PB-228 436

FLOURESCENT TRACING OF SEDIMENT IN COASTAL AREAS

Florida University
Gainesville, Florida

December 1967

DISTRIBUTED BY:

NTIS

National Technical Information Service
U. S. DEPARTMENT OF COMMERCE
5285 Port Royal Road, Springfield Va. 22151

PB 228 436

Reproduced by
NATIONAL TECHNICAL
INFORMATION SERVICE
U S Department of Commerce
Springfield VA 22151

ENGINEERING AND INDUSTRIAL EXPERIMENT STATION

College of Engineering

University of Florida

Gainesville

FLUORESCENT TRACING OF SEDIMENT IN COASTAL AREAS

TERMINAL PROGRESS REPORT
OF
RESEARCH GRANT WP-00057-04

Sponsored by:

Department of Health, Education, and Welfare

Submitted by:

University of Florida
Florida Engineering and Industrial Experiment Station
Coastal Engineering Department

December 1967

TABLE OF CONTENTS

	Page
LIST OF TABLES	iii
LIST OF FIGURES	iv
1. INTRODUCTION	1
2. INSTRUMENTATION AND OPERATIONAL SETUP	3
3 PRELIMINARY RESULTS ON MODES OF TRANSPORTATION	4
4. RESULTS FROM TESTS ON QUANTITY OF BED-LOAD TRANSPORT UNDER A VARIETY OF WAVE CONDITIONS	4
4.1 Bottom Profiles	4
4.2 No-bar Profiles, Test Conditions	5
4.3 Bar-trough Profile Test Conditions	6
4.4 General Results of Quantitative Tests	7
4.5 Comparison Between Results of Quantitative Tests	8
4.6 Particular Results from Test Nos. 16, 17 and 18	14
4.6.1 Tracer velocities (Figure 23)	14
4.6.2 Modes of transport	15
5. DIFFUSION ANALOGY OF SAND TRACER	20
5.1 Analysis of Results	24
5.2 Experimental Results	28
BIBLIOGRAPHY	31
APPENDIX	32

LIST OF TABLES

Table		Page
1.	List of Figures from Quantitative Tests	7
2.	Summary of Results from Quantitative Tests	10
3.	Peak Velocities of Tracers in Feet per Minute, Test No. 16	14
4.	Computation of Sheet Layer Thickness for 1 - 2 Hour Tests Corresponding to Figure 16 for Traps 2 and 3	17
5.	Sheet Layer Thickness, Test No. 17	18
6.	Grain Velocities up to Maximum Concentration for Test No. 18	19
7.	Results of Diffusion Analogy	30
8.	Equipment Expenditures for Sand Tracing Facilities	33

LIST OF FIGURES

Figure

1. Pier Installation, Fernandina Beach, Fla.
2. Bottom Profile, Test No. 4 (Berm)
3. Bottom Profile, Test No. 5 (Berm)
4. Bottom Profile, Test No. 17 (Berm)
5. Bottom Profile, Test No. 14 (Bar)
6. Bottom Profile, Test No. 16 (Bar)
7. Bottom Profile, Test No. 18 (Bar)
8. Injection and Sampling Setup, Test No. 4 (Berm)
9. Injection and Sampling Setup, Test No. 5 (Berm)
10. Tracer Injection Plan, Test No. 17 (Berm)
11. Injection and Sampling Setup, Test No. 14 (Bar)
12. Injection and Sampling Setup, Test No. 16 (Bar)
13. Injection and Sampling Setup, Test No. 18 (Bar)
14. Bed-load Transport Rate for Test No. 4 (Berm)
15. Bed-load Transport Rate for Test No. 5 (Berm)
16. Bed-load Transport Rate for Test No. 17 (Berm)
17. Bed-load Transport Rate for Test No. 14 (Bar)
18. Bed-load Transport Rate for Test No. 16 (Bar)
19. Bed-load Transport Rate for Test No. 18 (Bar)
20. Quantitative Results on All Tests on No-bar Profiles

Figure

21. Quantitative Results on All Tests on Bar/Trough Profiles

22. Longshore Drift as Function of Longshore Wave Energy

23. Mean Velocities for Tracer Grains

24. Quantity of Sediment Moving Past Pier in Form of Bed-Load and Suspended Load, Test No. 16

25. Development of Concentrations at Test No. 17

26. Development of Concentrations at Test No. 18

27. Comparison of the Semi-empirical Concentration Curve with the Actual Number of Green Tracers in Trap No. 3, Test No. 18, October 20, 1965

28. Determination of Longitudinal Dispersion Coefficient for Green Tracer for Test No. 18, October 20, 1965

29. Comparison of the Semi-empirical Concentration Curve with the Actual Number of Green Tracers in Trap No. 5, Test No. 19, February 2, 1966

30. Iso-lines of Blue Tracer Concentrations and Beach Profile Fernandina Beach February 11, 1966

FLUORESCENT TRACING OF SEDIMENT IN COASTAL AREA

1. INTRODUCTION

The last progress report of December, 1965 described the testing program and procedures. Preliminary results were outlined, together with a discussion of a diffusion analysis for littoral transport.

This report is the terminal progress report for U. S. Department of Health, Education, and Welfare (NIH) Grant WP-57. The project officially closed on March 31, 1966, but it is continued on another NIH grant, No. WP-00889-01.

This report describes some new results of testing and analysis including the difficulties encountered using an approach of the type indicated in previous progress reports. The principal objective, as originally stated in the proposal, is to contribute to the knowledge on the mechanics of sand transport in the littoral zone. The main results indicate patterns and give some ideas about quantity of littoral drift parallel to shore as determined from experiments at Fernandina Beach, located on the northeastern coast of Florida. This location was chosen due to the existing facilities, physical environment and history of information concerning littoral sand transport. The beach and nearshore bottom profile is typically multi-barred with a gentle slope of 2 - 3 percent. The sand has a

mean grain size of 0-2 mm. The mean tide range is 5.7 ft.

The correlation of littoral drift with wave and current conditions proved to be extremely difficult because of the problems in measuring currents in the surf zone in general, and particularly close to the bottom. Due to the rapidly changing current, many current meters are unsuitable because of their relatively slow response time. In addition, the quantity of suspended sediment is such that the proper operation of some meters is adversely affected. Until the first of the year, the Laboratory had located no device that could measure two components of current close to the bottom in the surf zone in two direction perpendicular to each other. This measurement is of vital importance as a determining parameter governing the amount of sand caught in a trap. An electromagnetic flowmeter has now been procured with the desired capability. This meter is being used on the continuation grant by the Department of Health, Education, and Welfare (No. WP-00889-01). The current meter is used adjacent to the mouth of each sand trap where water movement is measured at two directions perpendicular to each other (direction of wave propagation as well as longshore).

During 1965, two severe complications were encountered. One was that the level of contamination from previous fluorescent testing had increased to such a point that testing had to be postponed for two months, from November, 1965 to January, 1966. During this period, the Laboratory developed a satisfactory short-lived tracer which uses casein glue instead of resins to adhere the fluorescent dyes to the sand grains. Tests conducted showed that the use of casein glue did

not substantially alter the physical characteristics of the sand grains. By varying the amount of glue and the drying time of sand-glue-dye mixture, the time required for the dissolving of the dye coating can be varied from several weeks to several months. This tracer holds promise in solving the contamination problem for tests of this nature.

The second complication was loss of the helicopter, the only means of injecting tracer in the required short period of time. The closest alternate helicopter was more than 100 miles from the test site and the cost of chartering this craft was prohibitive. However, this helicopter was used for the last two tests, in order to make the most of the time available.

2. INSTRUMENTATION AND OPERATIONAL SETUP

The test setup and its instrumentation are described very thoroughly in the Progress Report of May, 1965. Figure 1 is a schematic of the pier installation at Fernandina Beach, Florida, showing the location of bed-load traps, suspended sediment traps and the wave and tide recorders. A total of six bed-load traps have been built to date to serve in the testing procedure. Because of the pioneer character of the work, entirely new instrumentation had to be developed. This included a scanning machine as described in Report No. 2, January, 1963, and a rather comprehensive operation system and new type bed-load trap as mentioned in detail in the Progress Report of May, 1965. A list of the major items of equipment purchased during this project is given in Appendix A.

3. PRELIMINARY RESULTS ON MODES OF TRANSPORTATION

As pointed out in previous reports, the tracer grains were to be used as velocity indicators, and from information gathered from the grains the modes of sand transport were to be ascertained. Most of the tests on modes turned out to be very complicated for meaningful analysis. It was found that there was often more variability in the samples of sand tracer from a given test than there was from the different tests under different conditions of waves and currents.

In addition to what has been mentioned in earlier reports, some additional results on modes should be mentioned in relation to the quantitative experiments described in Section 4.

4. RESULTS FROM TESTS ON QUANTITY OF BED-LOAD TRANSPORT UNDER A VARIETY OF WAVE CONDITIONS

4.1 Bottom Profiles

The most useful information gained from the research on this project are the data on quantity of bed-load drift at various locations in the littoral zone. Bed-load traps for each test were located a known distance from a baseline on the beach. For the most part, average wave conditions were sufficiently known; currents (or water velocities) at the pier, for the reason stated previously, were not in detail. Bottom topography along the pier and tide elevation were sounded for each test and thus the depth of water was always known.

Two basically different profiles were observed: (a) the berm type profile, Figures 2, 3, 4, which has a rather horizontal and shallow section just outside the MSL shoreline and (b) the bar and

trough profile, Figures 5, 6 and 7. The bar type profile is probably most predominant during the storm seasons (late fall, winter and early spring). This, however, does not mean that a bar is not always present, for it is probably more predominant during the winter season than during the summer season. During the summer the bar tends to flatten out and the trough fill in. A synopsis of specific tests is given below.

4.2 No-bar Profiles, Test Conditions

Test No. 4 was conducted 28 July, 1964. The test setup is shown in Figure 8. A total of 405 lbs. of tracers were dumped at a specified location south of the pier. The waves during the test had a significant height, H_s, of 40 cm, significant period, T_s, of 4 sec. and an angle of incidence of 30°*. The incident power due to the waves was computed from the significant wave conditions for the longshore wave power, P_l, and normal to shore wave power, P_v. These were computed to be 4.9 watts and 5.6 watts for P_l and P_v, respectively.

Test No. 5 was conducted 1 October, 1964, and the test setup is shown in Figure 9. Four hundred and fifty pounds of tracers were dumped on a line perpendicular to shore and 200 ft. south of the pier. The measured wave parameters were H_s equal to 140 cm, T_s equal to 4.5 sec. and an angle of incidence of 7°. The computed wave power components were a P_l of 32 watts and a P_v of 120 watts.

---

*The significant wave height is the average height of the highest one-third waves; the significant wave period is the average period of the highest one-third waves.

Test No. 17 was conducted 3 November, 1964. Figure 10 shows the test setup. One hundred and twenty pounds of tracers were dumped at a single point located 200 ft. south of the pier. The waves had a significant height of 45 cm, a T_s of 4.5 sec. and an angle of incidence of 5°. The computed power components were P_l equal to 1.5 watts and P_v equal to 9 watts.

4.3 Bar-trough Profile Test Conditions

Test No. 14 was conducted 19 January, 1965. Figure 11 shows the test setup. This test was to measure the quantity of sand transport and no tracer material was used. Wave activity was H_s equal to 46 cm, T_s equal to 4 sec. and an angle of incidence of 45°. The computed wave power gave a P_l of 5.7 watts and P_v of 8.1 watts.

Test No. 16 was conducted 16 April, 1965. Six hundred pounds of tracer material were dumped as indicated in Figure 12. H_s was equal to 100 cm, T_s was equal to 5.8 sec. and the angle of incidence was 20°. The computed wave power components were a P_l of 32 watts and P_v of 60 watts.

Three bed-load traps (Nos. 2, 3, 4) and one suspension load trap were operated. Station 1 could not be operated because of the shallow depth, and there was only suspension load recorded at suspension load Station 2S, which was close to wave breaking. No load was recorded in the other suspension traps.

Test No. 18 was conducted 20 October, 1965. The test setup is shown in Figure 13. Tracers of five different colors were dumped at a distance of 200 ft. in an arc of 120° with the center at

Station 3. Two sectors of 30° closest to the pier were left without tracers. The measured wave activity was H_s equal to 60 cm, T_s equal to 8 sec. and an angle of incidence of 20°. P_l and P_v were computed to be 44 and 130 watts, respectively.

4.4 General Results of Quantitative Tests

Figures 14 - 19 give results of the quantitative tests.

The results refer to two different types of profiles - the "no-bar profile" and the "bar-trough profile."

Results of the two different types of profiles are tabulated below, splitting up into results from low-energy tests and high-energy tests. The results from these tests are mentioned in the following paragraph where results from various tests are compared (see Table 1). Some particulars on modes of transport are mentioned in Section 4.6 as part of an attempt to explain some details of the movement of material on the bottom surface.

TABLE 1

LIST OF FIGURES FROM QUANTITATIVE TESTS

		No-Bar Type			Bar-Trough Type		
		#4	#5	#17	#14	#16	#18
Low Energy	Profile	2		4	5		
	Quantities	14		16	17		
High Energy	Profile		3			6	7
	Quantities		15			18	19

In Test 17 (Fig. 4), the bottom profile is actually a bar-trough profile, although it is not very developed as such. The wave action is so minimal, however, that this profile could never demonstrate bar-trough characteristics with respect to longshore drift quantities, and has been included as having no-bar characteristics.

4.5 Comparison Between Results of Quantitative Tests

Figure 20 shows the results of three tests on no-bar profiles, that is, profiles where there was no bar within the test section when it was flattened out and without any clear tendency toward the development of a bar. From Figure 20, it may be seen that for the same longshore energy, the nearshore records (traps) have higher transport than the offshore records for the same actual depths. This is probably caused by wave breaking on the beach and the following uprush which causes considerable stir-up of material in the nearshore zone. The importance of the longshore energy for longshore drift is also evident from Figure 20.

Figure 21 shows the results of three tests on bar profiles -- profiles with a clear bar formation or tendency toward the same. From Figure 21, it may be seen that for the same longshore energy, the nearshore records (traps) have most transport when the 5 ft. depth is considered for low energy and when 10 ft. depth is considered for high energy. It is also true, however, that records from 10 ft. depth generally speaking are highest, and that records from 15 ft. depth in the trough demonstrate higher transport than records from 15 ft. depth on the bar. This emphasizes the importance of transport as bed-load in the trough by longshore current

for the relatively mild wave conditions of which we are speaking. The longshore current may mainly be tidal in this case where no wave breaking took place on the bar, as evidenced by the fact that nearshore transport (10 ft.) exceeds bar transport (15 ft.). It is also evident that longshore drift increases with longshore energy.

Table 2 is a resumé of the results of three tests on no-bar and three tests on bar profiles. Distinction is made between low energy and high energy results. Figure 22 depicts the results.

Table 2 clearly demonstrates that the nearshore (5 ft. depth) transport is much larger than the transport at greater depth for the wave conditions of which we are speaking here, when H_s < 100 cm. This situation is particularly true for the no-bar profile and for low energy. For higher energy, the situation develops that the transport increases considerably nearshore as well as in the trough and bar section of the profile, which now becomes "active for transport" thanks to the higher energy input, possibly assisted by tidal currents which help to transport material longshore. From the above mentioned, we may also come to the conclusion that more scattering of data may be expected for the bar-trough profiles than for the no-bar profiles.

Comparison of Figures 15 and 19 (no-bar and bar-trough profiles) in particular reveals the most pronounced difference in drift attitude between no-bar and bar-trough profiles. While in the no-bar profile drift decreases with increase in depth, the opposite seems to be the case in the bar-trough profile. A maximum

TABLE 2

SUMMARY OF RESULTS FROM QUANTITATIVE TESTS

Low Energy		Type of Profile							
		No-Bar Drift in Grams per Minute			Bar Drift in Grams per Minute				
Test No.	P_1/P_v	Depth ft.	Location		Test No.	P_1/P_v	Depth ft.	Location	
			Nearshore	Offshore				Nearshore	Offshore
4	5/6	5	10-50	1-5	14	6/8	5	3-4	
		10	1-3				10	5	
17	1.5/9	5	(50-70)				15 (bar)		0.5-2
		10	0.5-8	1-7			17 (trough)		0.5-1.5
		15	0.5-3						
		20	0.1-0.3						
High Energy									
5	32/120	5	30-90	10-20	18	44/130	5	-	
		10	5-20				10	50-80	3-5
							15 (bar)		5-20
							18 (trough)		50
					16	32/60	5	-	
							10	20	4-5
							15 (bar)		8-11
							18 (trough)		15-25

transport still occurs closest to shore. A second maximum of almost equal magnitude occurs in the trough (Figs. 7 and 19, St. 3), while on the bar transport is least. This is undoubtedly caused by the fact that in this case there were no waves breaking on the bar but a rather strong current (1-2 ft. per sec.) in the trough. This current, however, may have been partly tidal.

It is also apparent that the transport in the 10 to 15 ft. depth interval (St. 2, 3) for the bar-trough profile is stronger than the drift in the 5 to 10 ft. interval for the no-bar profile (St. 2, 3). The traps installed at Stations 2 and 3 carried in both cases most load in the bar-trough profile. The longshore wave powers increased from 32 to 44 from no-bar to bar-trough profile, which could only account for the about 40% increase in transport according to energy flux. Tidal currents as mentioned above may have an influence on this result.

A very interesting similarity between the transport rates in the two kinds of profiles is noted by the increase of transport with depth in the single point of sampling (Figs. 14 - 19). This is particularly true for the bar-trough profile, but is also recorded at Stations 2 and 4 in the no-bar profile. This may be explained by an increase in longshore current velocity with depth. Inasmuch as these currents are caused by wave action and have their maximum value in the deep part of the trough in a bar-trough profile and just inside the breaking point in a no-bar profile, it could be expected that with wave action under a small angle with the shoreline, the influence of the longshore current on the drift would be very

important in the bar-trough profile because waves have decreased less by refraction and are almost perpendicular to the shoreline, for which reason the stir-up effect is at its maximum. This effect decreases with depth, but a few feet variation in depth is of little importance. An increase of the velocity of the longshore current which carries the material alongshore therefore is very important. With a greater angle of incidence, the wave heights decrease more and the decrease of stir-up effect with depth becomes important. The velocity of the longshore current increases, but the drift is probably mainly distributed in accordance with the stir-up effect of the oscillating wave motion.

With respect to the no-bar profile, an increase in depth causes an increase in wave action on the nearshore parts of the profile, therefore an increase in longshore drift as long as the point considered is close to the breaking point of the waves and not outside the breaking point. This again particularly is true for small angles of incidence of the wave action, while for increasing angles of incidence the wave motion in the nearshore zone decreases, and the influence of depth on the stir-up is restricted to a smaller area. In this case the decrease in drift which starts just outside the breaker zone happens in a narrower section of the profile, thanks to the smaller wave heights.

Another explanation for the phenomena registered is that normal tidal currents increase with depth from shore until a certain limit and their influence on longshore drift becomes important. In the nearshore zone at Fernandina Beach, such tidal currents, apparently mixed with concentrations of wind-driven currents, occur

in the nearshore zone and may have made their contribution to the above-mentioned results.

This subject was not investigated in detail, but it is planned to observe currents at the pier during no-wave conditions during the continuation of the study.

Figure 22 is a graph relating longshore transport to longshore energy. From this graph it may be seen that:

(1) Longshore transport increases with longshore energy. Not enough results are available to draw any conclusions, and all results refer to bed-load in narrow areas only.

(2) The importance of a longshore current superimposed on the wave-energy current may be seen for the low-energy section.

(3) The importance of the longshore currents combined with the stir-up may be seen from the results for the higher energy level. The perpendicular-to-shore component of the wave energy is twice as high for the 44 watt longshore case as for the 32 watt and results bear witness hereof.

(4) The importance of the longshore current is also evident from the trough transport predominance over bar transport for the energy levels we are considering. This is undoubtedly going to change for higher input of wave energy, with frequent wave breaking on the bar.

4.6 Particular Results from Test Nos. 16, 17 and 18

4.6.1 Tracer velocities (Figure 23)

Test no. 16, Figure 23 shows the mean velocity of grain migration recorded during the first 1 - 2 hours of the test.

From Figure 23 (Bar profile, Figure 6) and from Table 3, it appears that peak velocities of grains are fastest for movements parallel to the wave crests. Mean velocities show more uniform modes. Unfortunately, it was not possible to measure the sand movement at trap no. 1 located closest to shore.

The reason for the relative distribution of velocities of sand grains should probably be sought in the interaction between the longshore current and the asymmetrical water motion associated with the shallow water wave as it approaches the shore. Some material is mainly pushed toward the shore and some other is mainly carried away from shore by the oscillating water motion.

TABLE 3

PEAK VELOCITES OF TRACERS IN FEET PER MINUTE

Test no. 16, Figure 6		
Direction of Wave Propagation	Mean Maximum Speed Recorded	Average Speed 1-2 hours
deviate 50°	4	4
deviate 60°	5	5
deviate 80°	7	2
deviate 100°	9	5
deviate 110°	88	5
deviate 120°	7	5

Certain concentrations of currents tend to carry water longshore at higher velocities (usually occurring at the middle of the trough). This explains qualitatively the velocity pattern found. It should still be remembered that the number of traps was too limited and distributed only on one line perpendicular to shore.

Test No. 18, Figure 23 (bar profile), shows a somewhat similar pattern in the way that maximum velocities seemed to occur for directions close to and parallel with the wave crests. The longshore current close to bottom is material laden and in this case may seek towards a rip current carrying water (and material) seaward.

Test No. 17, Figure 23 (no-bar profile), in this case, shows the highest recorded velocity occurred for the direction closest to the direction of wave propagation probably a result of the low swell action and the absence of a longshore current caused by wave breaking outside the uprush zone.

4.6.2 Modes of transport

Test No. 16, Figure 24 (bar profile), shows the development of concentrations. Tides were increasing when this test was run and this situation is clearly reflected in the results of the quantitative tests.

At the start of the experiments, material load was strongest as suspension at Station 2S (traps closer to shore could not be operated). As the tide increased, suspension load at Station 2S decreased while bed-load transport increased at Stations 3 and 4, and it became possible to measure bed-load

at Station 2.

Test No. 17, Figure 25 (no-bar profile), shows the development of concentration at Stations 1, 2, 2S, 3 and 4 as a function of time.

Accumulation in Station 4 was an irregular process, while accumulation in Stations 1, 2 and 3 (2S) developed normally with a fast-developed peak after which concentrations dropped slowly.

Although the drift was small at Stations 2 and 3, an attempt was made to compute certain details of the bed-load transport in the surface layer. The velocities corresponding to peak concentrations are indicated in Table 4, from which it may be seen that maximum velocities now were relatively highest in the direction of wave propagation.

The following reasoning is designed only to get an idea on the thickness of the migrating sheet layer.

With n grains trapped per unit of time, one has with V_x = travel velocity of grains, b = thickness of the bed-load layer, w = width of trap and k a material constant which indicates the volume each grain occupies (including actual volume of solid mass plus voids):

$$w \cdot b \cdot V_x = nk_1$$

or

$$b = nk_1/wV_x = k_2 \cdot n/V_x \quad (k_2 = k_1/w)$$

With 0.18 - 0.22 mm grains, and w = 15¼ in., one has

$$k_1 \sim 0.5 \cdot 10^{-5} \text{ cm}^3$$

and

$$k_2 \sim 10^{-7} \text{ cm}^2$$

$$B = \sum_{n=1}^{n=j} N/n_{max}\ k_2(nj/V_j)$$

or

$$B/k_2 = \frac{N}{n_{max}} \sum_{j=1}^{j=j\ max} \frac{ni}{V_j} = \frac{N}{maxD} \sum_{j=1}^{j=j\ max} n_j t_j$$

when t_j is the time intervals considered.

TABLE 4

COMPUTATION OF SHEET LAYER THICKNESS FOR 1-2 HOUR TESTS
CORRESPONDING TO FIGURE 16 FOR TRAPS 2 and 3

Trap no.	j	D(ft)	Δt (min)	V_j (ft/min)	$\frac{n_{total}}{time}$	n_j	N/n_{max}	n_j/V_j	B_{total}/k_2
2	1	241	35	6.9	948/15	63.2	92.5	9.2	
	2		65	3.7	1828/15	122		32.9	
	max		95	2.5	1010/15	67.3		26.5	
								68.6	6350
3	1	200	35	5.7	1/15	0.067	2790	0.012	
	2		55	3.6	65/15	4.33		1.19	
	max		75	2.7	57/15	3.80		1.43	
								2.63	7330

The corresponding B and mean velocity are listed in Table 5, which also gives the thickness in number of grains of 0.2 mm.

TABLE 5

SHEET LAYER THICKNESS. TEST NO. 17

	Station 2	Station 3
B (mm)	0.0064	0.0073
Number of 0.2 mm grains thick	$\frac{1}{35}$	$\frac{1}{30}$

Considering as a first approximation a 1 meter wide bottom area for Station 2, one has for the quantity of littoral drift, Q:

$$Q = 60^2 \cdot (100) \cdot 0.00064 \cdot (4.2 \cdot \frac{30}{60})$$

$$= 480 \text{ cm}^3 = 0.48 \text{ liters per hour}$$

For a 40 cm wide trap, the quantity is 0.17 liter per hour,

$$= 170 \cdot 1.8/60 = 5 \text{ grains per minute,}$$

which is an average figure corresponding to Figure 16.

Test No. 18 - The development of concentrations at Station 3 is shown in Figure 26, disregarding an initial contamination of relatively minor order from an earlier test.

Table 6 indicates the average velocity of grains for the period until maximum concentration occurred.

TABLE 6

GRAIN VELOCITIES UP TO MAXIMUM CONCENTRATION FOR TEST NO. 18

Color	Average maximum velocity (feet/minute)	Total number of grains	Total weight grams/minute
Green	2	700	
Yellow	1.7	400	
Red Orange	1.4	300	18
Red Violet	1.7	200	
Blue	—	0	

From Figure 26 it may be seen that the maximum velocity of grain movement recorded was almost parallel to the wave crests (swells) and that the velocity in the direction of wave propagation was the smallest velocity.

The average accumulation for the period up to maximum concentration was 18 grams per minute. The average thickness, B, of the sheet layer may be computed from the equation:

$$B \cdot 40 \text{ cm} \cdot 54 \text{ cm}/60 = 18 \text{ grams}/1.8 \cdot 60$$

$$B = 1/200 \text{ cm} \sim \frac{1}{20} \text{ mm} = 0.05 \text{ mm}$$

= 1/4 grain, which is a reasonable figure.

5. DIFFUSION ANALOGY OF SAND TRACER

The movement of tracer sand in the littoral zone is analogous to the diffusion of a contaminant in a fluid. The general diffusion equation can be derived from the equation of continuity, assuming that the mixture of sand and water can be treated as an incompressible fluid. The sand movement can be treated as a continuum in that the mean free path of individual sand particles is much smaller than the significant lengths involved in the problem. If it is assumed the sand movement is also a stationary process and can be averaged over some vertical distance between depth of no motion to a height of no tracer particles, the diffusion equation reduces to a two-dimensional problem. Assuming a gradient type diffusion where D_x and D_y are the longitudinal and lateral dispersion coefficients, the expression for tracer concentration C, averaged over time and vertical can be written as:

$$\frac{\partial C}{\partial t} + u \frac{\partial C}{\partial y} + v \frac{\partial C}{\partial y} - D_x \frac{\partial^2 C}{\partial x^2} - D_y \frac{\partial^2 C}{\partial y^2} = 0 \qquad (1)$$

where u and v are velocity components in the x and y horizontal directions. This is the general advective-diffusion equation in two-dimensions. The complete derivation has been given previously in Reference (6).

The dispersion coefficients, D_x and D_y, have been assumed constant. The assumption of constant dispersion coefficients is generally only applicable in cases where the size of the eddies, i.e. scale of turbulence, causing the mixing, is small compared to the dimensions of the tracer patch. This seems a reasonable assumption, if we consider

that almost all the energy of the system is in the frequency band of the waves and that the orbital path of the waves is representative of the eddy size.

In the solution of equation (1), an instantaneous point source of tracer concentration is assumed, which corresponds to the dropping of tracers at point in the experiment. This imposes the condition that as time, t, tends to zero, the concentration tends to zero at all points except at the origin where it becomes infinite.

Transferring to a (ζ, η) space defined by

$$\frac{x}{D_x^{\frac{1}{2}}} = \frac{\zeta}{p^{\frac{1}{2}}}; \quad \frac{y}{D_y^{\frac{1}{2}}} = \frac{\eta}{p^{\frac{1}{2}}}$$

where

$$P = (D_x D_y)^{\frac{1}{2}}$$

we get $dxdy = d\zeta d\eta$ and

$$\frac{u}{D_x^{\frac{1}{2}}} = \frac{U}{p^{\frac{1}{2}}} ; \quad \frac{v}{D_y^{\frac{1}{2}}} = \frac{V}{p^{\frac{1}{2}}}$$

where U and V are velocities in (ζ, η) space corresponding to u and v respectively. Hence, concentration, C, at (x,y) transfers to the same concentration at (ζ, η). Equation (7) becomes

$$\frac{\partial c}{\partial t} + U \frac{\partial c}{\partial \zeta} + V \frac{\partial c}{\partial \eta} - P\left[\frac{\partial^2 c}{\partial \zeta^2} + \frac{\partial^2 c}{\partial \eta^2}\right] = 0 \qquad (2)$$

Using the transformations

$$C(\zeta, \eta, t) = Z(\zeta, \eta, t) e^{\frac{1}{2}(U\zeta + V\eta)} \qquad (3a)$$

and

$$Z(\zeta, \eta, t) = \Phi(\zeta, \eta, t)e^{-\frac{P}{4}(U^2 + V^2)t} \tag{3b}$$

Equation (2) simplifies to

$$\frac{\partial \Phi}{\partial t} - P\left[\frac{\partial^2 \Phi}{\partial \zeta^2} + \frac{\partial^2 \Phi}{\partial \eta^2}\right] = 0 \tag{4}$$

This is recognized as the same equation applicable to the diffusion of heat in a solid. Many solutions to this equation for various initial and boundary conditions are in the literature. The reader is referred to "Conduction of Heat in Solids" by H. S. Carslaw and J. C. Jaeger which probably gives the most complete coverage in one source of the various solutions to equation (4).

Considering the case of an instantaneous point source at (ζ, η) and $t = 0$, the solution of equation (4) as given by Carslaw and Jaeger is

$$C = \frac{K_{xy}}{t} e^{-\frac{1}{4Pt}\left[\zeta^2 + \eta^2\right]} \tag{5}$$

Transforming back to the (x,y) space the solution of equation (2) is

$$C = \frac{K_{xy}}{t} \exp -\left[\frac{(x - \bar{u}t)^2}{4D_x t} + \frac{(y - \bar{v}t)^2}{4D_y t}\right] \tag{6}$$

This solution can be verified by substitution into the diffusion equation of the partial derivatives of equation (6) that are required. A discontinuity exists at the origin for $t = 0$, but this presents no

problem in the physical interpretation. The solution is applicable to diffusion from a point source at diffusion rates that are not necessarily the same in both coordinate direction. The diffusivity may therefore be inhomogeneous and anisotropic.

A property of equation (6), considering center line conditions, is that the time-concentration curve is skewed at small x and that the time-concentration curve tends to become a normal distribution curve at large x.

A transformation of equation (6) into a normal form can be made by substituting

$$\sigma_x = \sqrt{2D_x t} \tag{7a}$$

$$\sigma_y = \sqrt{2D_y t} \tag{7b}$$

from which is obtained

$$C = K_{xy} 2\pi \sqrt{2D_x}\sqrt{2D_y} \frac{e^{-\frac{1}{2}\left[\frac{x-\bar{u}t}{\sigma_x}\right]^2}}{\sqrt{2\pi\sigma_x}} \frac{e^{-\frac{1}{2}\left[\frac{y-\bar{v}t}{\sigma_y}\right]^2}}{\sqrt{2\pi\sigma_y}} \tag{8}$$

Since the total area of the normal bi-variate distribution is

$$\iint_{-\infty}^{+\infty} \frac{e^{-\frac{1}{2}\left[\frac{x-\bar{u}t}{\sigma_x}\right]^2}}{\sqrt{2\pi\sigma_x}} \frac{e^{-\frac{1}{2}\left[\frac{y-\bar{v}t}{\sigma_y}\right]^2}}{\sqrt{2\pi\sigma_y}} \, dy \cdot dx = 1 \tag{9}$$

Therefore, by integrating over the entire area of the tracer spread, the entire tracer per unit length M is obtained

$$M = K_{xy} 4\pi \, (D_x D_y)^{\frac{1}{2}} \tag{10}$$

and

$$K_{xy} = \frac{M}{4\pi(D_x D_y)^{\frac{1}{2}}}$$

Making this substitution, gives concentration expressed in ppm as

$$C = \frac{M}{2\pi\sigma_x\sigma_y} \exp - \tfrac{1}{2}\left(\left[\frac{x-\bar{u}t}{\sigma_x}\right]^2 + \left[\frac{y-\bar{v}t}{\sigma_y}\right]^2\right) \qquad (11)$$

5.1 Analysis of Results

The experimental setup for tracer studies is explained in Reference 4. Six sand traps are placed along a pier. The tracer is introduced updrift of the pier. It is assumed that all tracer particles arriving at the sand traps are trapped and later counted. Thus, the concentration, or total number of tracer particles, over the width of the sand trap and over an interval of time, can be determined.

It can be seen from equation (11) that the maximum concentration occurs when

$$x = \bar{u}t \quad \text{and} \quad y = \bar{v}t$$

Thus, the mean velocities $\bar{u}$ and $\bar{v}$ are determined when the peak concentration occurs.

The coordinate system is arranged so that the mean direction of flow is in the x direction. This is usually parallel or nearly parallel to the beach, i.e., line of traps. Since the mean flow is in the x-direction, flow in the y-direction is zero, $\bar{v} = 0$.

For concentration along the center line of mean flow, y = 0, the concentration is expressed as

$$C = \frac{M}{2\pi\sigma_x\sigma_y} \exp^{-\frac{1}{2}\left[\frac{x-\bar{u}t}{\sigma_x}\right]^2} \qquad (12)$$

Setting

$$\sigma_x = \sqrt{2\ D_x t}$$

and taking the log of equation (18) gives

$$\text{Log } Ct = \text{Log } \frac{M_z^2}{2\pi\sigma_x\sigma_y} - \frac{(x-\bar{u}t)^2}{4D_x t} \log e \qquad (13)$$

By plotting equation (13) on semi-log graph paper it is seen that it plots as a straight line, and the slope of the line is given by

$$\text{slope} = \frac{\log e}{4D_x}$$

In this manner the longitudinal dispersion coefficient can be determined.

The advantage of using this method is that the actual initial concentration of the tracer need not be known, for only the relative concentrations are important.

Setting x = ut, when $C = C_{max}$, in equation (13), it is seen that

$$C\Big|_{t=\frac{x}{u}} = C_{max} = \frac{M}{4\pi(D_x D_y)^{\frac{1}{2}}} \frac{x}{u}$$

Thus, equation (13) can be rewritten as

$$C = \frac{C_{max}}{t} \frac{x}{u} e^{-\frac{1}{2}} \frac{(x-\bar{u}t)^2}{2D_x t} \qquad (14)$$

and a comparison between the experimental results and the semi-empirical curve can be made.

It was found in some of the experiments that the results obtained did not correspond well to the mathematical model of the dispersion from an instantaneous point source. It can be seen in Figure 1 that the semi-empirical curve describes the experimental results fairly well up to the peak concentration, but thereafter the concentrations do not decay to zero as proposed in the model. This may be due to two causes: the tracers dropped at a point do not correspond to an instantaneous point source, or that the tracers may be intermittently buried and uncovered.

The general solution of the diffusion equation for a source that is a function of time, as opposed to an instantaneous point source, has the form

$$C = \frac{1}{4(\pi K)^{\frac{1}{2}}} \int_0^t \Phi(t) \frac{e^{-\frac{1}{4Kt}(x^2 + y^2)}}{t^{\frac{1}{2}}} \, dt \qquad (15)$$

This distribution of tracer concentration is due to a continuous point source of strength $\Phi(t)$ from $t = 0$ onwards. By selecting the correct source function $\Phi(t)$, the semi-empirical curve can be made to fit the data in Figure 1 very well. This was attempted, but found to give results that could be given no physical interpretation. In any event, the analysis of dispersion coefficients

is only dependent on the data to the peak of the curve. What happens after the peak concentration has passed does not affect the calculations of D_x and D_y.

The tracer dropped on the bottom may be intermittently buried and uncovered. This could result in data similar to Figure 1. Therefore, it is important that the test duration be long enough to assure that the time of peak concentration is measured, for this determines the mean velocity of the sand movement.

The lateral dispersion coefficient, D_y, can be found by calculating the variance in the y direction as a function of time where

$$\sigma_y = (2tD_y)^{\frac{1}{2}} \tag{16}$$

Denoting increment values for specific time by subscript i, the variance is equal to

$$\sigma_{yi}^2 = (2t_i \cdot D_y) = \frac{\sum_{o}^{i=n} y^2 C_i - \frac{\sum_{o}^{i=n} (yC_i)^2}{\sum_{o}^{i=n} C_i}}{\sum_{o}^{n} C_i} \tag{17}$$

By plotting σ_{yi} vs. $(2t_i)^{\frac{1}{2}}$ the slope of the line is given as $(D_y)^{\frac{1}{2}}$, and the lateral dispersion coefficient can be calculated.

5.2 Experimental Results

The longitudinal dispersion coefficient, D_x, was determined by plotting equation (13) on semi-log paper. An example is shown in Figure 28, where the slope of the line was calculated by the least-square method. The test of the assumption of a constant dispersion coefficient is that the points plot as a straight line. As can be seen in Figure 28, the points are fairly linear and thus the assumption is valid to at least a first degree of approximation.

Figures 27 and 29 are examples showing the semi-empirical curve as calculated by equation (14), superposed on the observed data. In Figure 27, it can be seen that the theoretical curve fits the observed fairly well to the peak, but thereafter does not, as previously discussed. Figure 29 is an example where the theoretical and observed curves more closely match, and the assumption of an instantaneous point source seems applicable.

The lateral dispersion coefficients were calculated using equation (17). The results of experiments analyzed to date using the diffusion analogy are presented in Table 7. D_y varied over an order of magnitude from 0.014 to 0.265 ft^2/sec, whereas the ratio of D_y/D_x was fairly uniform varying only from about 0.1 to 0.4. In all cases the lateral dispersion coefficient was less than the longitudinal coefficient. It appears from the tracer studies that although the transversal sand movement is much more violent than the littoral sand movement, the net transversal movement

is less.

The isolines of concentration are reconstructed as a typical example in Figure 30. The bottom profile is also shown. It can be seen that the tracers move along the crest of the bar and that there is little exchange across the trough. This was typical of the experiments where the tracers either predominantly moved along the crest of the bar or were transported adjacent to the beach. The trough acted as a barrier to transversal exchange of sand from offshore to onshore or vice versa. Imposing boundaries on transversal movement violates the assumption of a constant lateral dispersion coefficient. It should be remembered that the assumption of constant dispersion coefficients is in the sense that they are averaged over the time scale of the experiments. Thus, the calculated values of D_y should be valid to at least a first approximation.

TABLE 7

Z*	D_x	D_y	D_y/D_x	$\bar{u}$	$\bar{v}$	α	T	H_s	U
14.5	0.38	0.08	0.21	0.032	0.021	4°	6	3.0	0.33
8.0	1.03	0.13	0.13	0.045	0.045	4	6	3.0	0.33
13.5	0.68	0.26	0.39	0.039	0.000	4	6	3.0	0.33
14.5	0.53	0.17	0.33	0.044	0.015	4	6	3.0	0.33
10.5	0.50	0.00	0.00	0.050	0.027	3	6	3.0	1.10
10.5	0.77	0.00	0.00	0.029	0.023	3	6	3.0	1.10
14.5	0.45	0.12	0.27	0.033	0.017	4	6	3.0	0.33
14.0	0.12	0.014	0.12	0.017	0.009	10	9	4.0	0.09

*Z - mean depth of water (ft)

D_x - longitudinal dispersion coefficient (ft^2/sec)

D_y - lateral dispersion coefficient (ft^2/sec)

$\bar{u}$, $\bar{v}$ - mean velocity of tracer movement in x and y directions (ft/sec)

α - wave angle of incidence

T - average wave period (sec)

H_s - significant wave height (ft)

U - mean velocity of littoral current at water surface (ft/sec)

BIBLIOGRAPHY

1. Carslaw, H. S. and Jaeger, J.C. Conduction of Heat in Solids, Oxford University Press, 1947.

2. De Vries, M. Discussion of Paper "Sand Transport Studies with Radioactive Tracers" by David W. Hubbell and William W. Sayre, Proceedings, ASCE, 91, No. HY1, January, 1965.

3. Diachishin, A. N. Dye Dispersion Studies, Proceedings, ASCE, 89, No. S.A. 1, January, 1963.

4. Gaither, W. S. and McGill, J. A. Field Testing Methods and Equipment Used at Fernandina Beach for the Tracing of Littoral Drift, Department of Coastal Engineering, University of Florida, May, 1965.

5. Kalkanis, G. Transportation of Bed Material Due to Wave Action, Coastal Engineering Research Center, Tech. Memo. No. 2, February, 1964.

6. Thornton, E. B. Diffusion of Sand Particles in the Ocean from a Point Source, Coastal Engineering Department, University of Florida, November, 1965.

APPENDIX A

The use of fluorescent sand tracers has become a very useful engineering tool. Much of the pioneering work in this area, particularly with application to the surf zone, has been accomplished here at the University of Florida. Since most of the work was unique, it required many innovations and the acquisition of considerable new equipment. Much of this equipment was purchased during the course of this project, and the major expenditures are listed in Table 8.

TABLE-8-

EQUIPMENT EXPENDITURES FOR SAND TRACING FACILITIES

Item	Vendor	Purchase Price
CAPITAL EQUIPMENT:		
Hanovia Lamps with Accessories (2)		$ 391.86
Mixer (a)		
Mixer (b)		
Sieving Machine (sizing)	Russell Constructions	1,725.46
Grinding Machine	Christy & Norris	1,181.73
Ro-Tap Sieve Shaker (sieve analysis)	Test Lab Corporation	570.00
Oven (25%)	Forma Scientific	238.75
Scanning Machine		8,967.00
Photomultiplier (23%)		1,120.00
Crane		507.04
X/Y Recorder (33 1/3%)		637.66
Microvoltmeter		519.20
Visual Accumulation Tube Sand Size Analyzer (35%)		212.62
Minor Lab Equipment		1,000.00
Stevens Water Level Recorder (2)		950.68
MANUFACTURED EQUIPMENT:		
Bed-load Traps (5)		$4,000.00
Suspension Pipe Line Traps (3)		1,200.00
Pipe Line Installation at Pier		2,500.00
Pumps		1.026.00

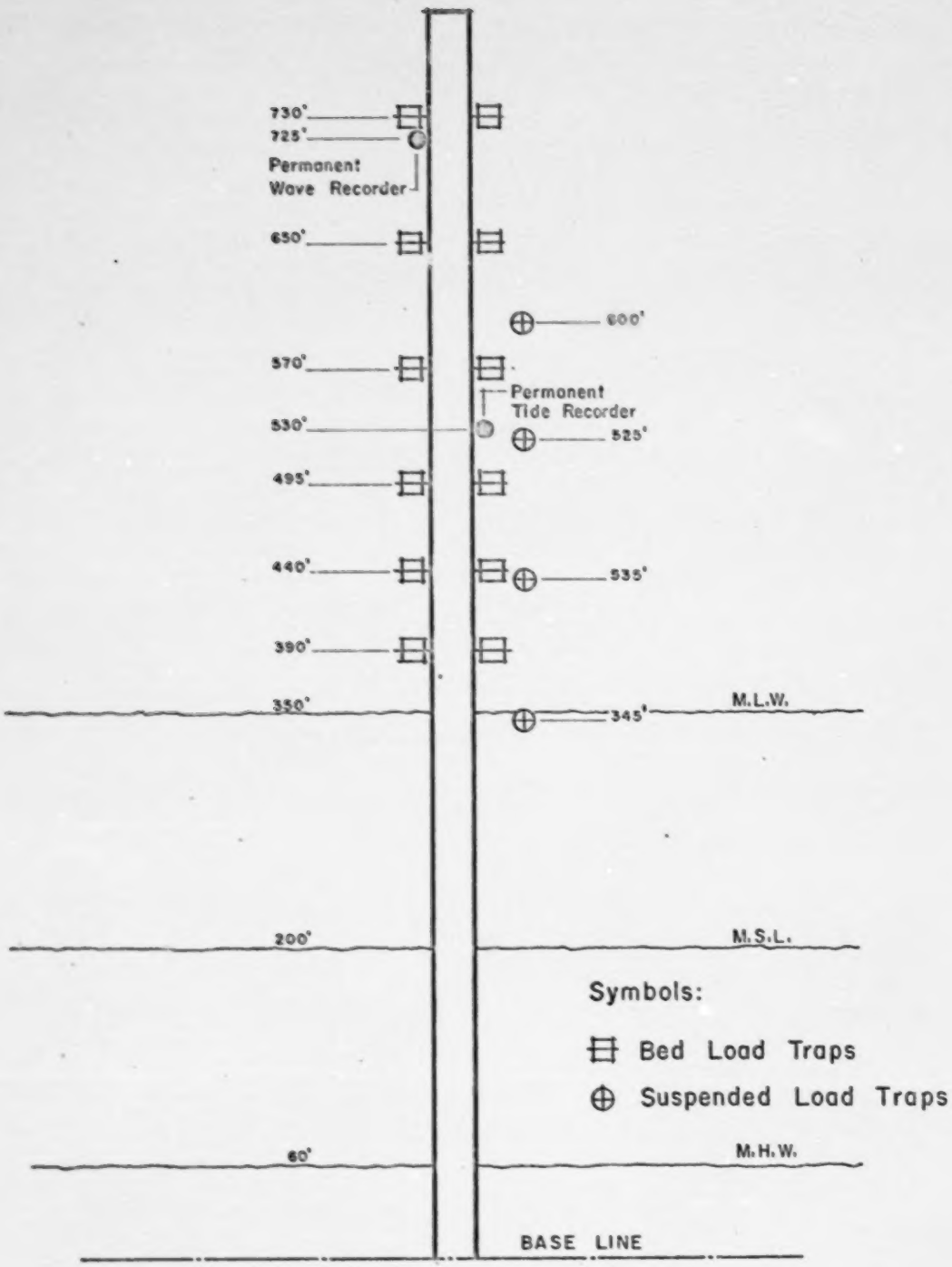

FIG. 1

PIER INSTALLATION, FERNANDINA BEACH, FLORIDA

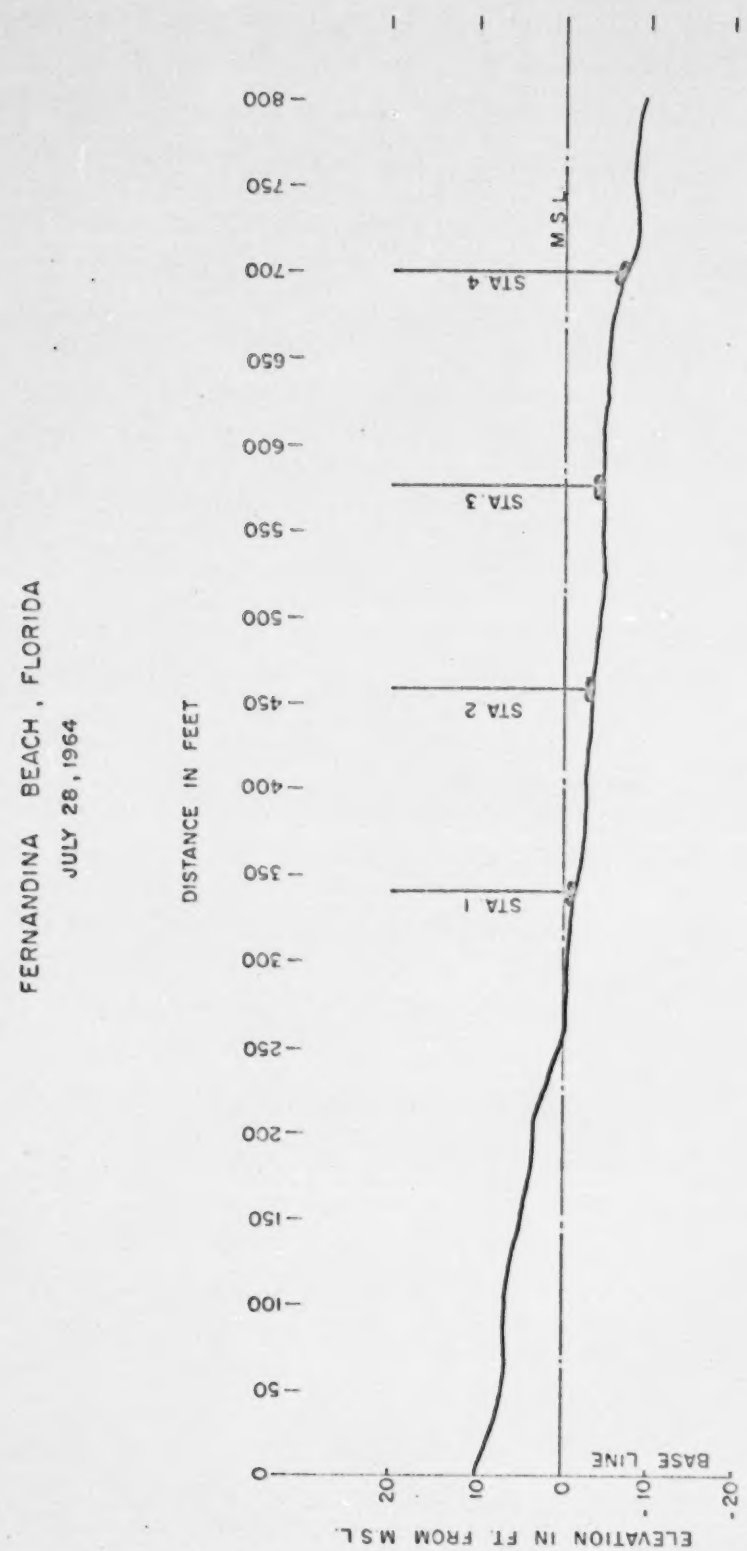

FIGURE 2 BOTTOM PROFILE, TEST NO. 4 (berm)

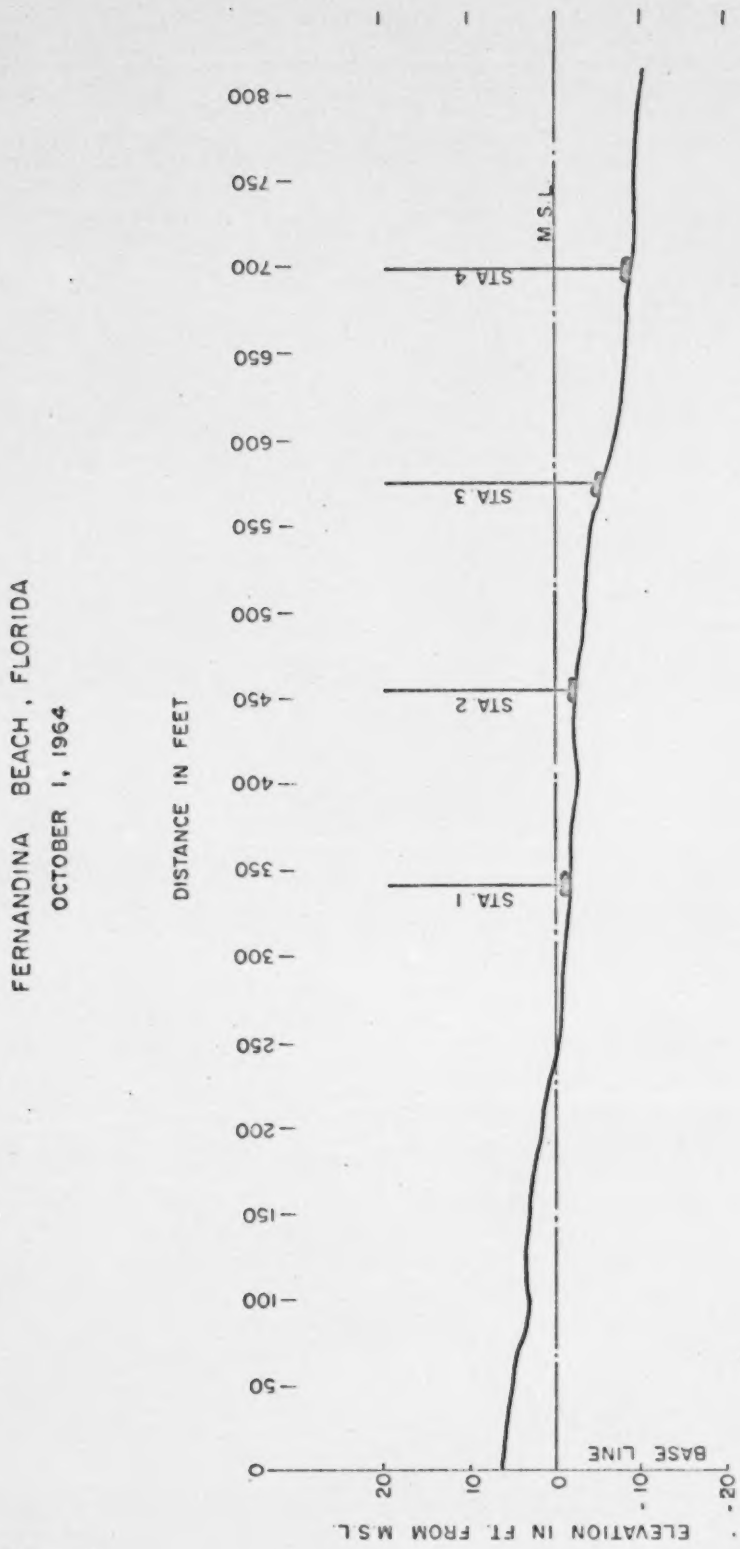

FIGURE 3 BOTTOM PROFILE FOR TEST No 5 (berm)

FERNANDINA BEACH, FLORIDA
MAY 13, 1965

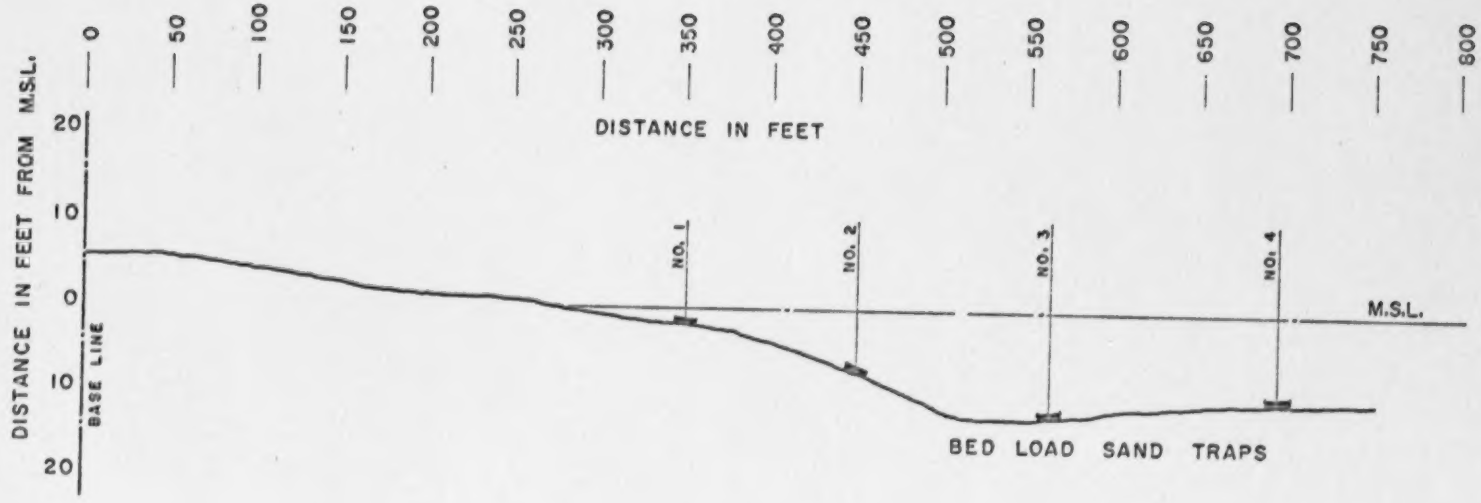

FIGURE 4 BOTTOM PROFILE, TEST NO. 17 (berm)

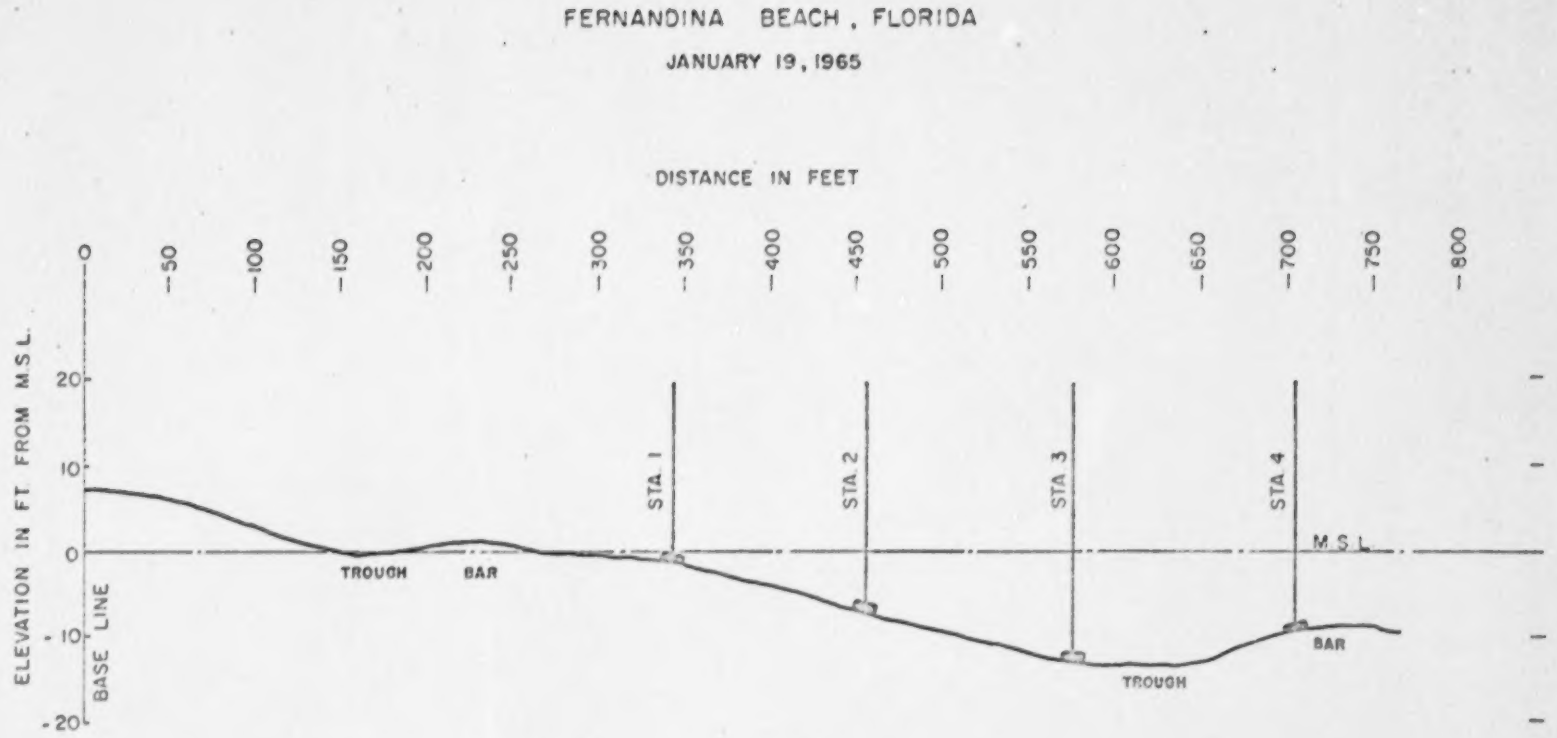

FIGURE 5 BOTTOM PROFILE FOR TEST Nº 14 (bar)

SIXTEENTH FLUORESCENT TRACER EXPERIMENT

FERNANDINA BEACH, FLORIDA

APRIL 14, 1965

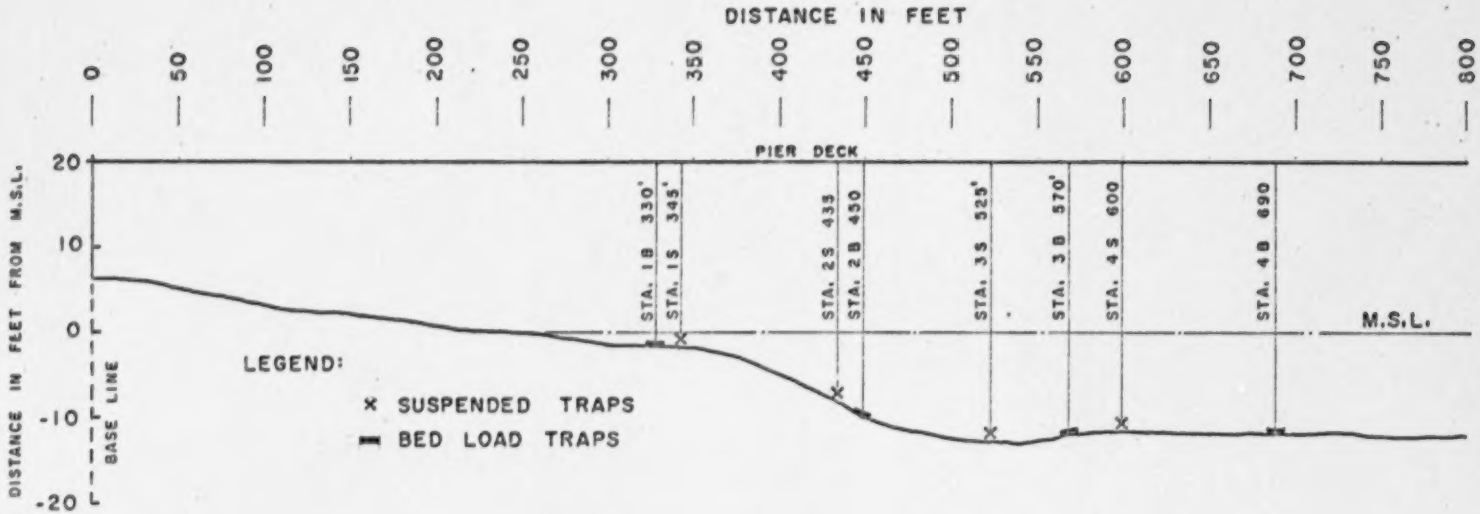

FIGURE 6 BOTTOM PROFILE, TEST NO. 16 (bar)

FERNANDINA BEACH, FLORIDA
OCTOBER 20, 1965

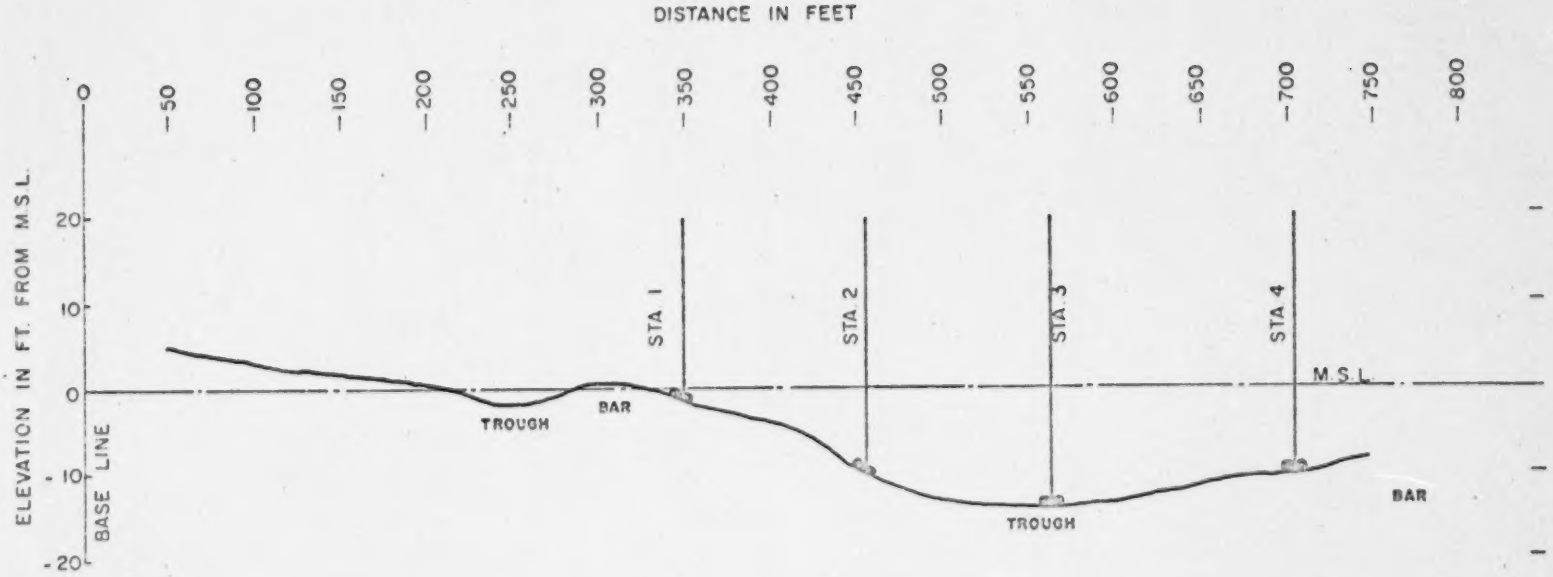

FIGURE 7 BOTTOM PROFILE - TEST Nº 18 (berm)

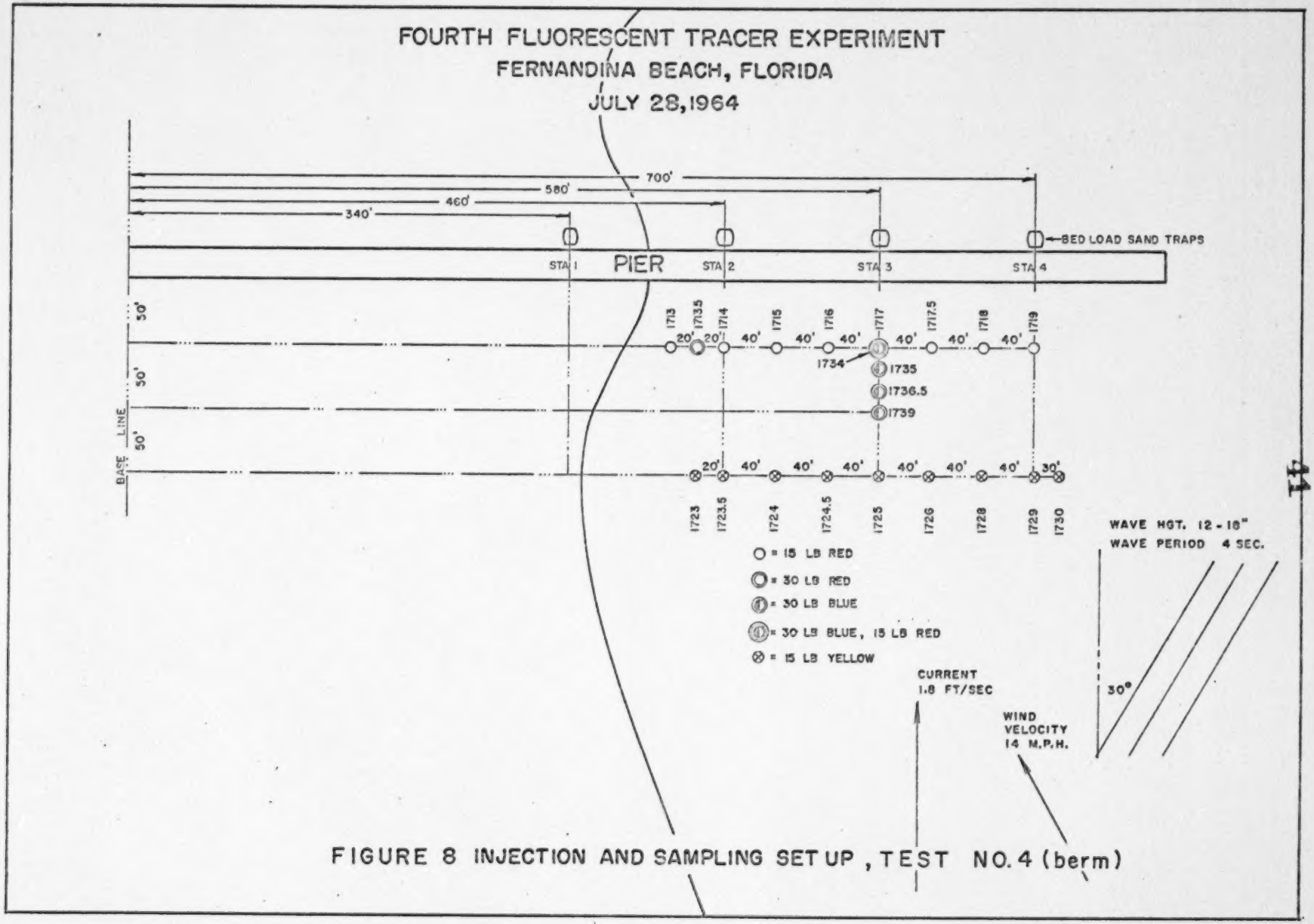

FIGURE 8 INJECTION AND SAMPLING SET UP, TEST NO. 4 (berm)

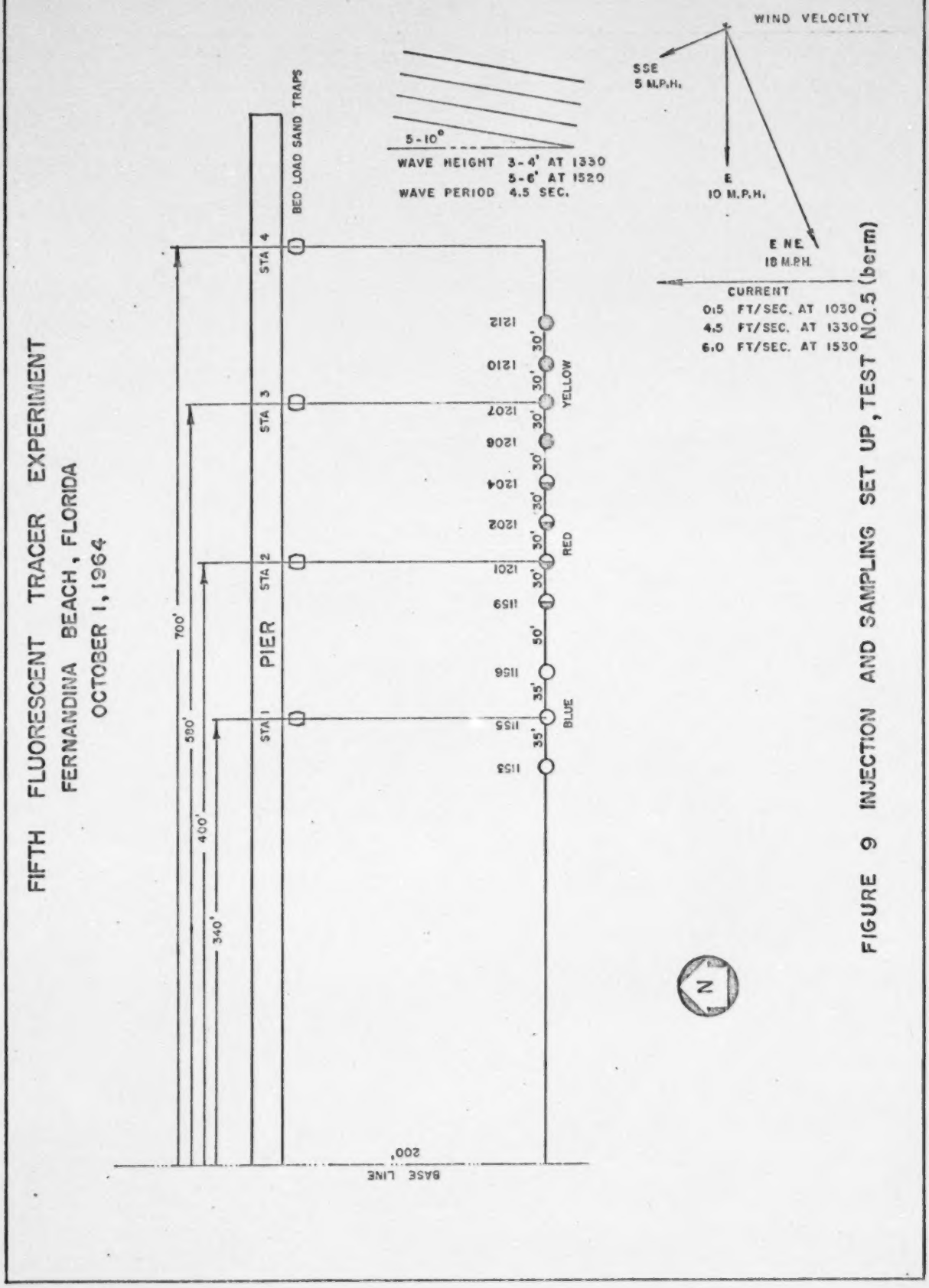

FIGURE 9 INJECTION AND SAMPLING SET UP, TEST NO.5 (berm)

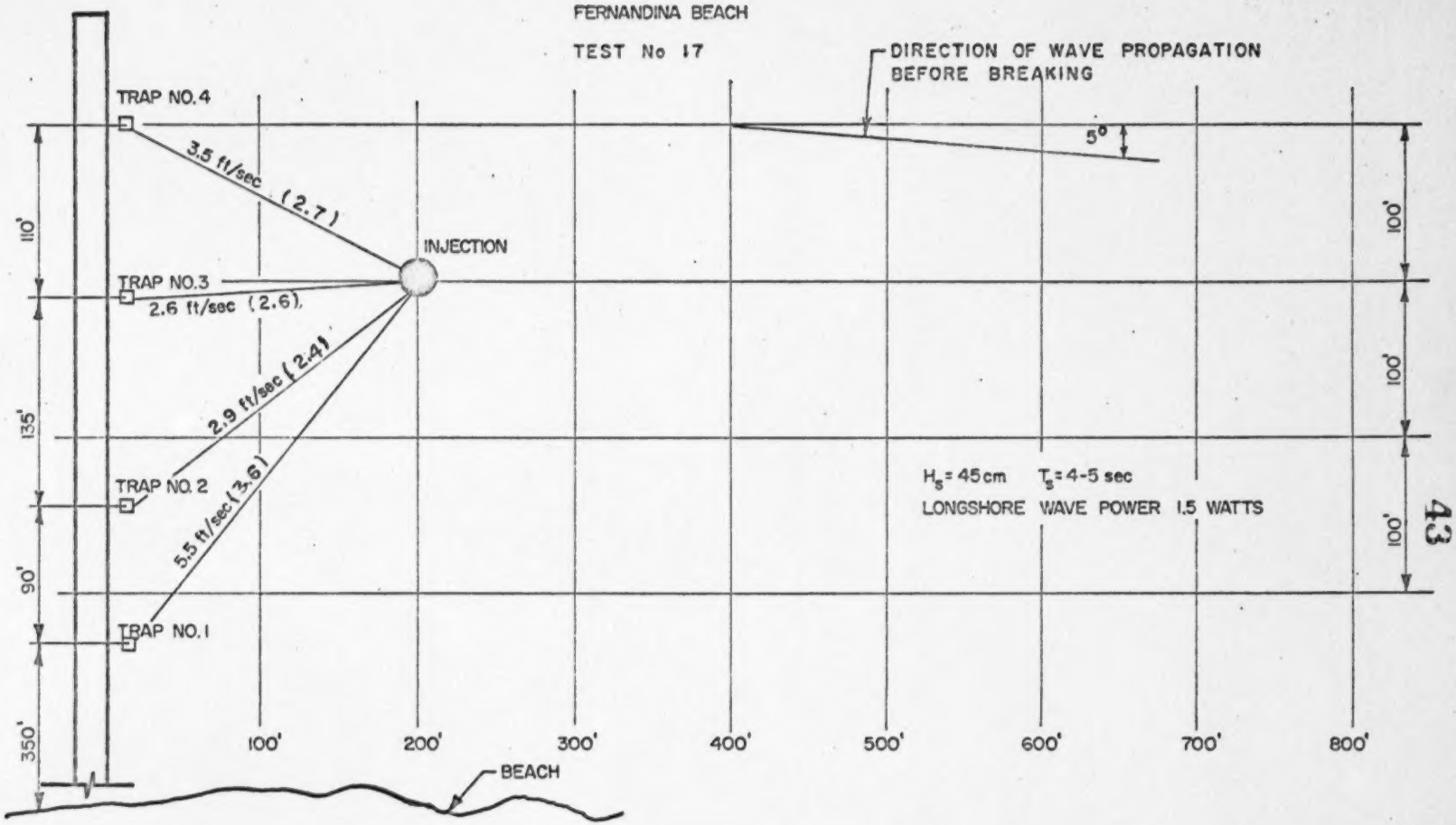

FIGURE 10 TRACER INJECTION PLAN, TEST NO. 17 (berm)

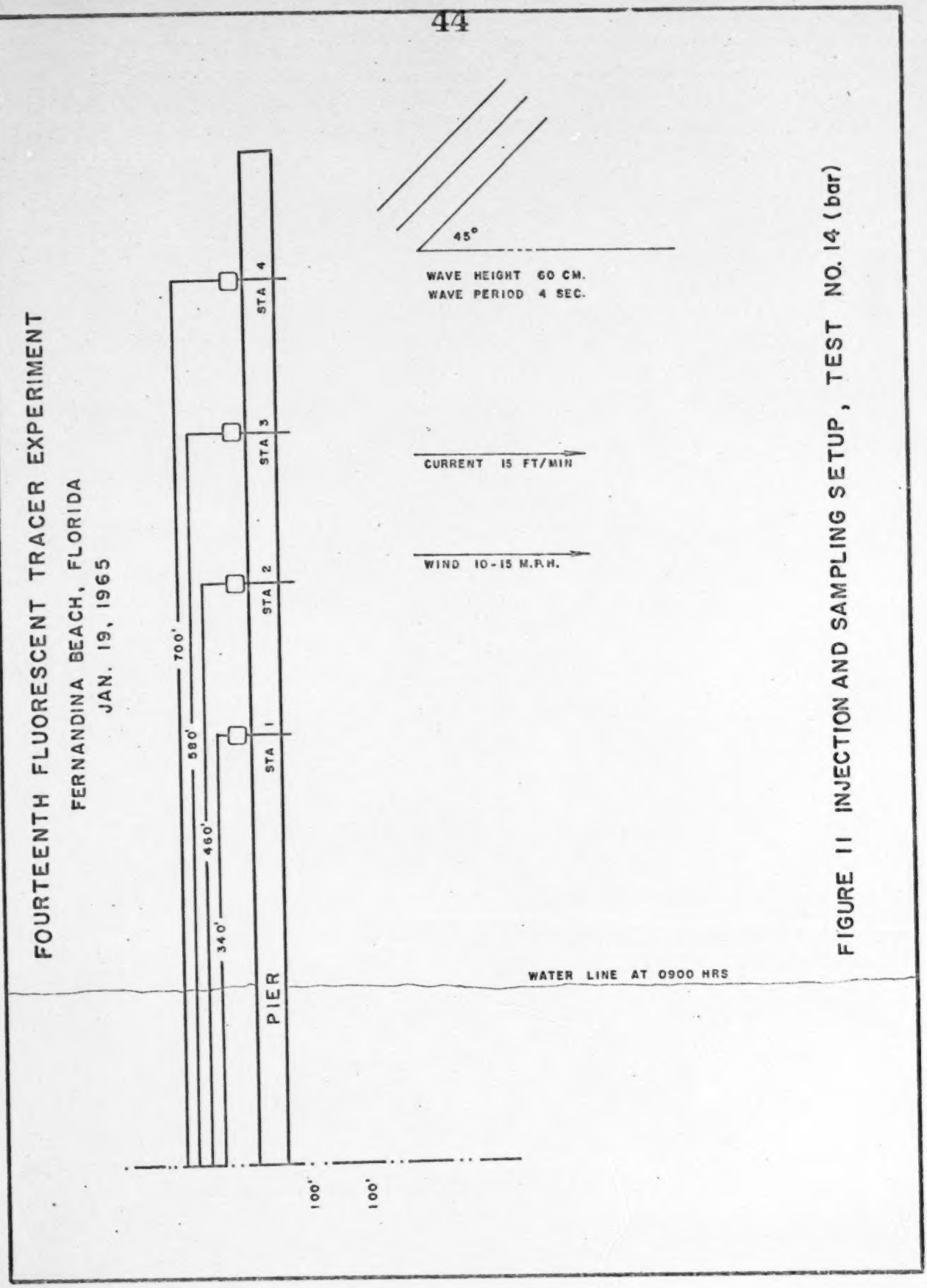

FIGURE 11 INJECTION AND SAMPLING SETUP, TEST NO. 14 (bar)

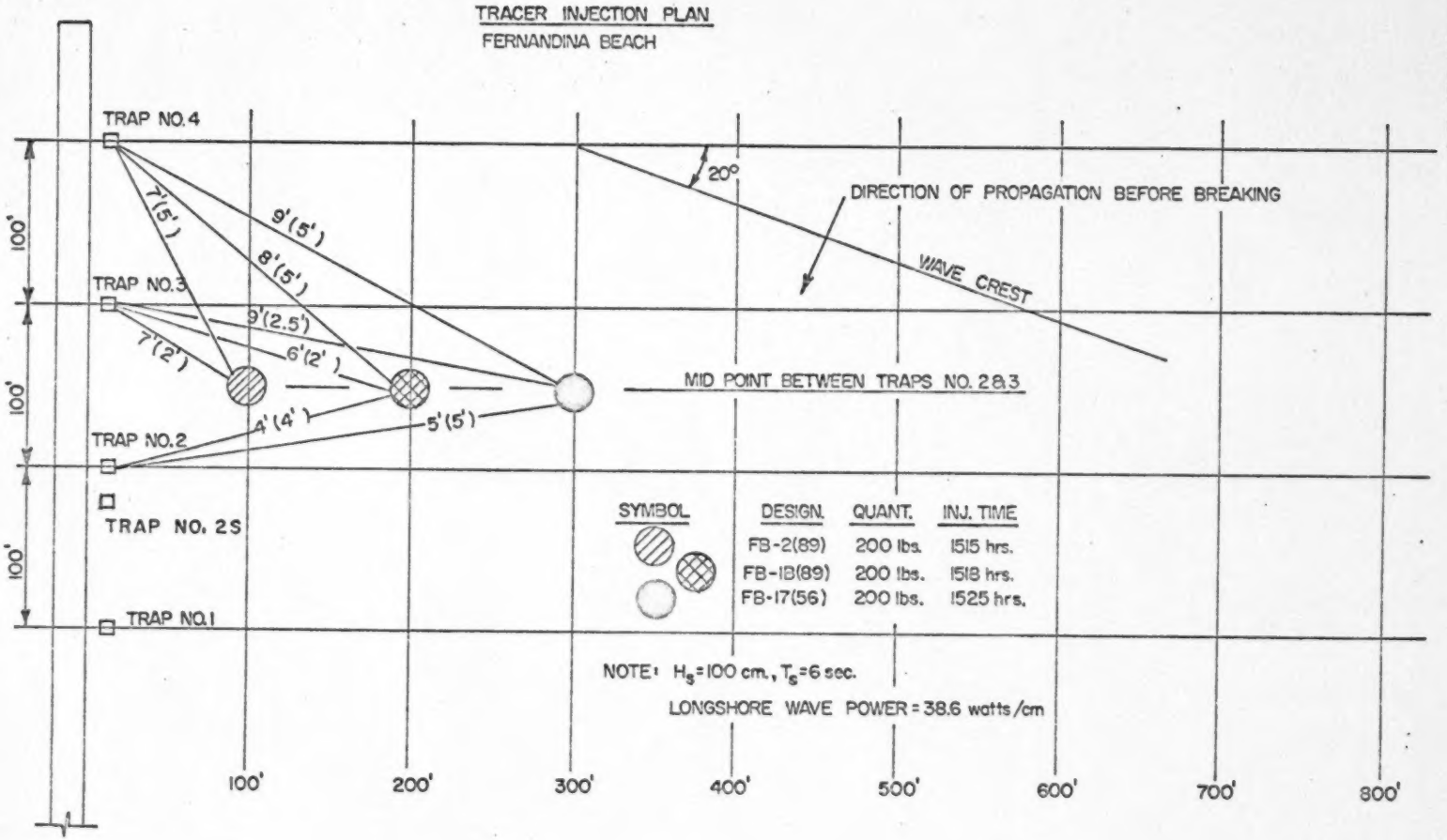

FIGURE 12 INJECTION AND SAMPLING SET-UP, TEST NO.16(bar)

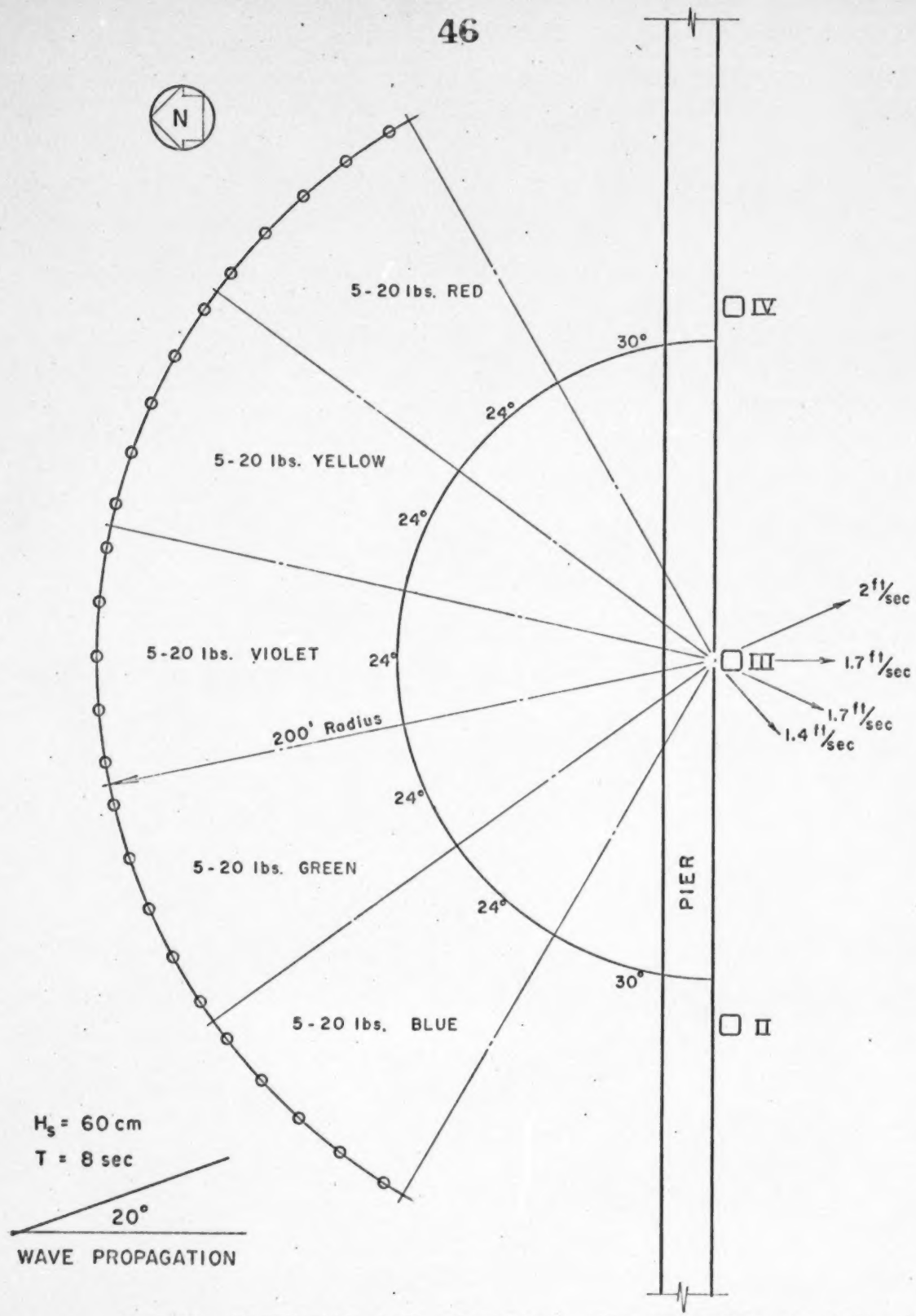

Fig. 13: INJECTION AND SAMPLING SET-UP TEST NO. 18 (bar)
FERNANDINA BEACH, FLA.

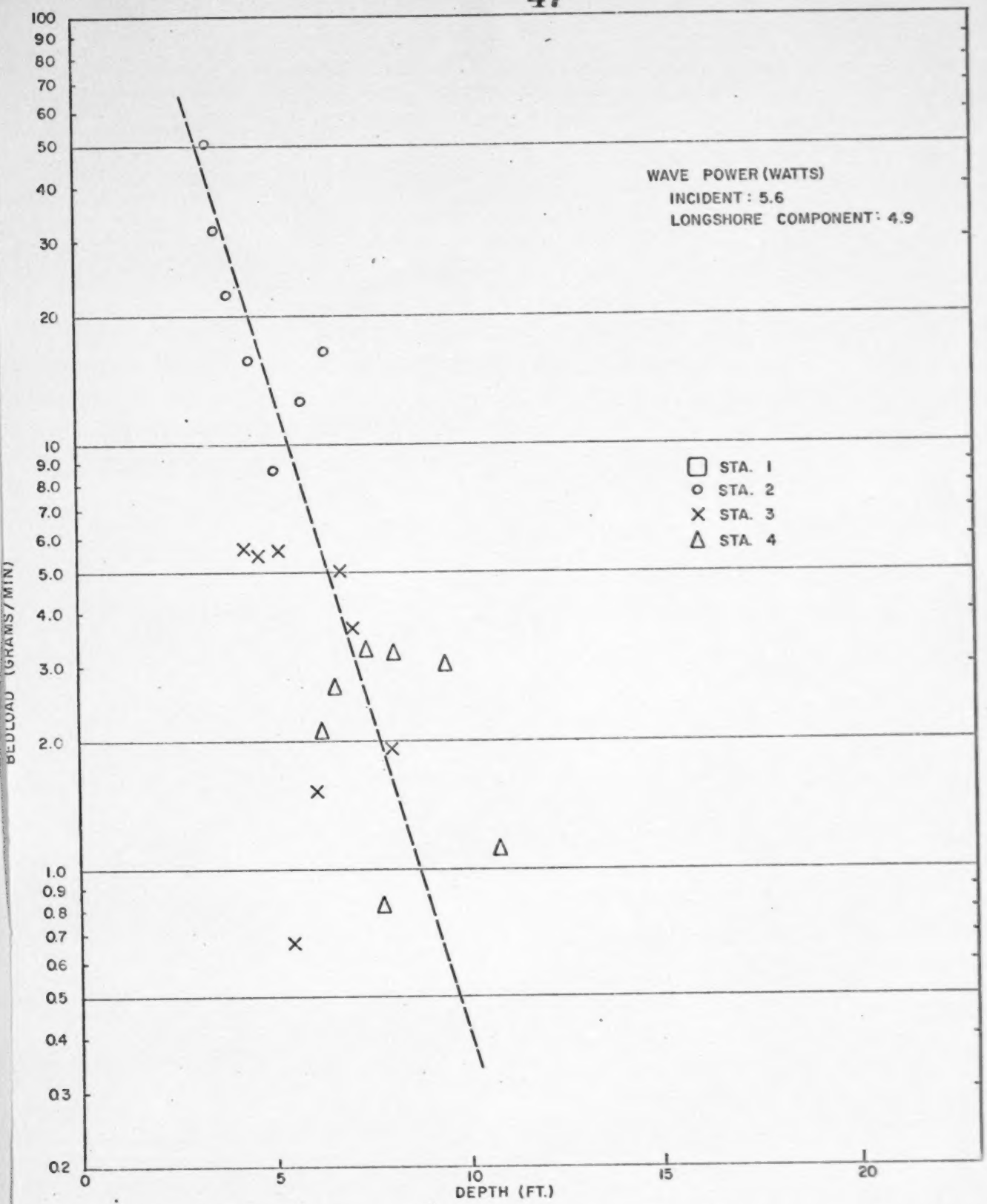

FIGURE 14 BEDLOAD TRANSPORT RATE FOR TEST NO. 4 (berm)
JULY 28, 1964

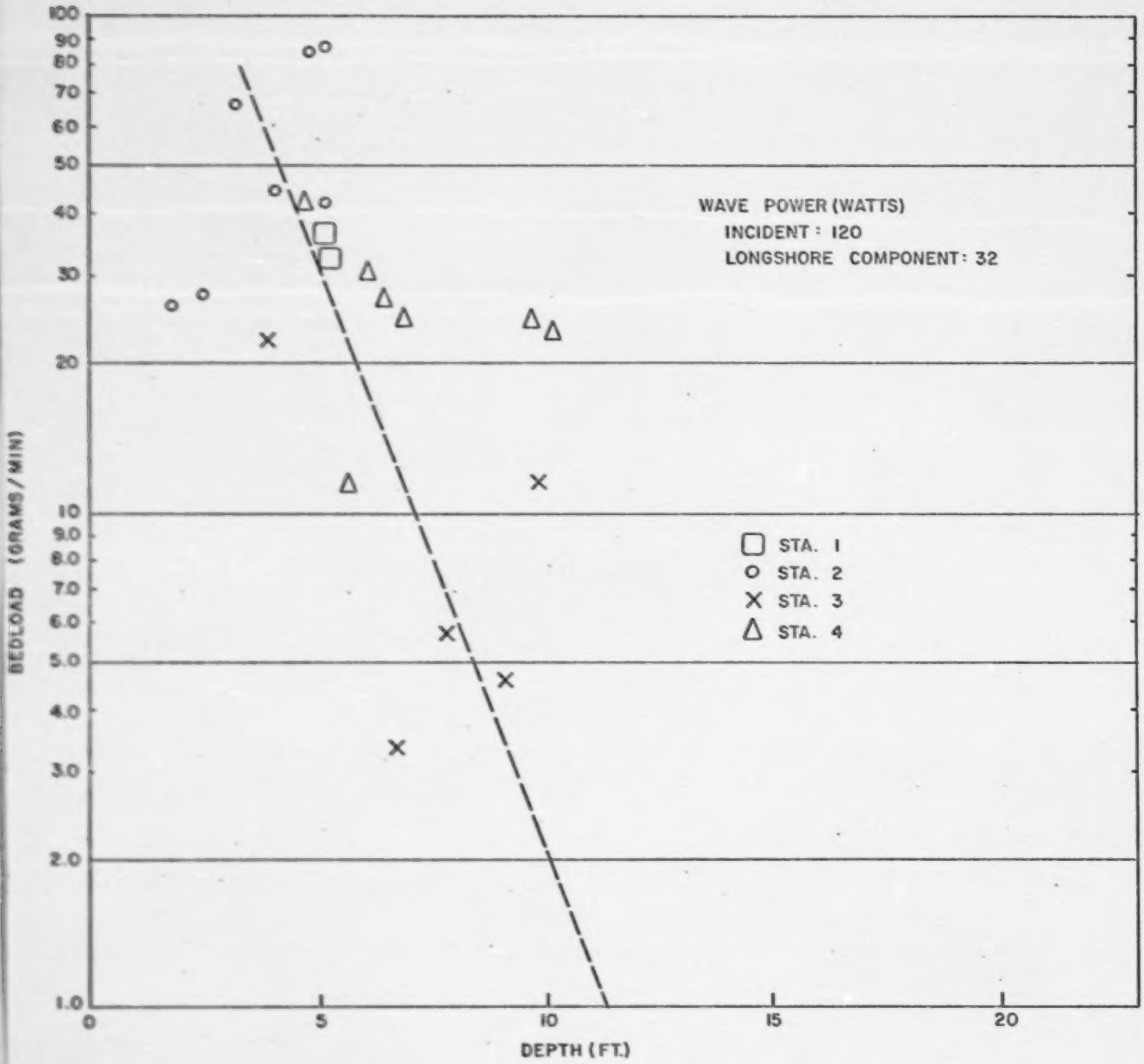

FIGURE 15 BEDLOAD TRANSPORT RATE FOR TEST NO. 5 (berm)

OCTOBER 1, 1964

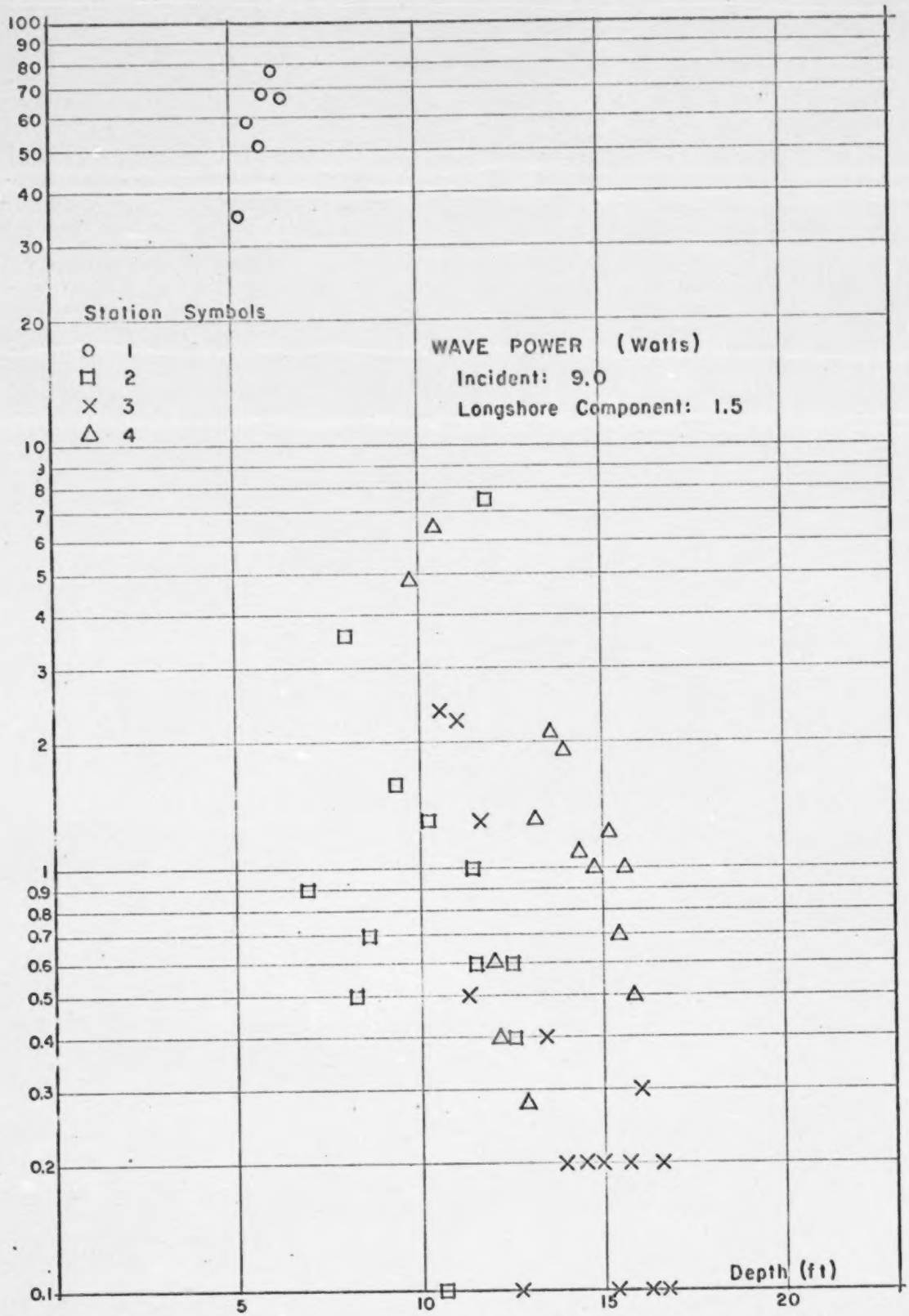

FIGURE 16 BED LOAD TRANSPORT RATE FOR TEST NO. 17 (berm)

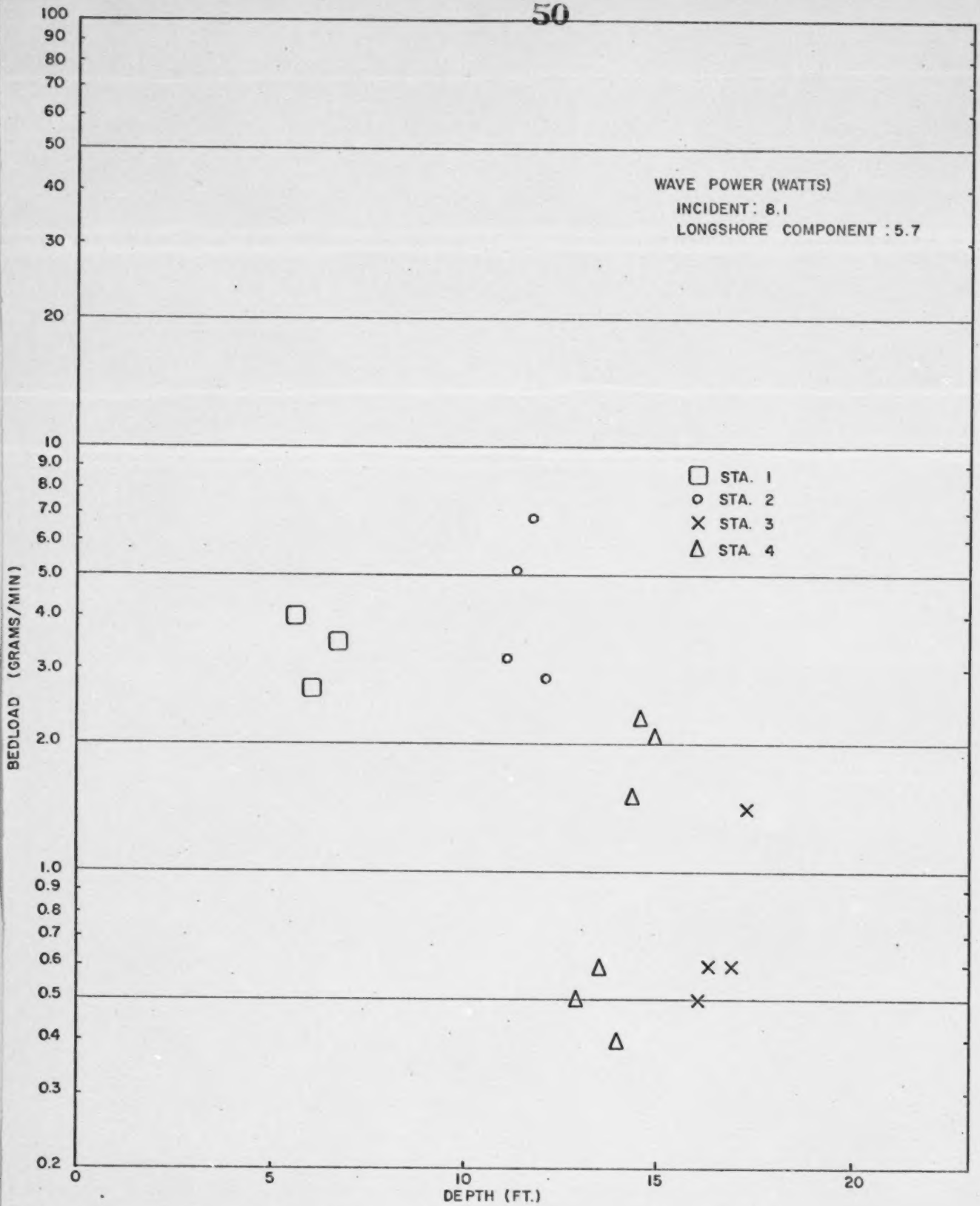

FIGURE 17 BEDLOAD TRANSPORT RATE FOR TEST NO. 14 (bar)
JAN 19, 1965

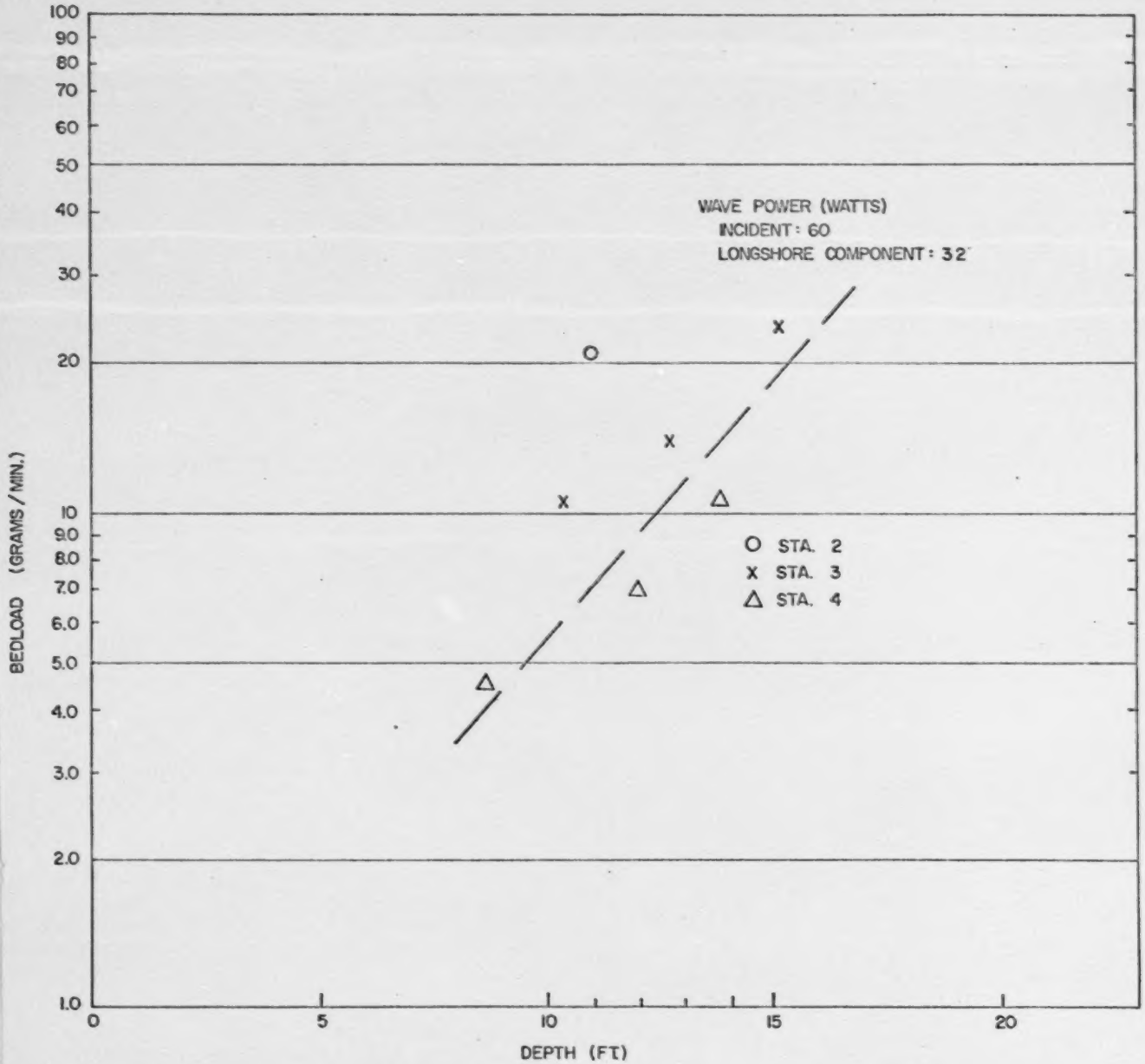

FIG. 18: BEDLOAD TRANSPORT RATE FOR TEST NO. 16 (bar)

APRIL 14, 1965

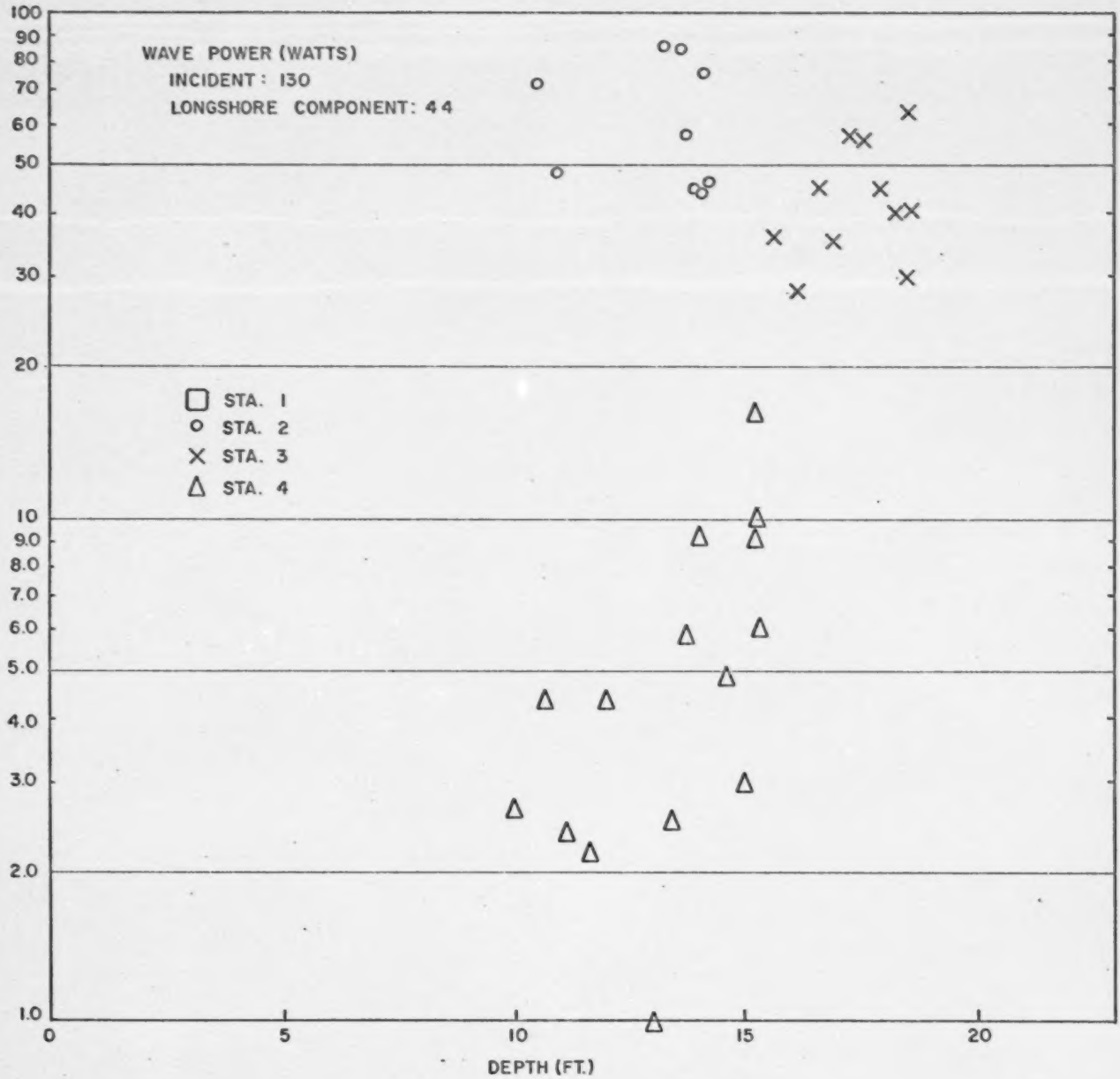

FIGURE 19: BEDLOAD TRANSPORT RATE FOR TEST Nº 18 (bar)

OCTOBER 20, 1965

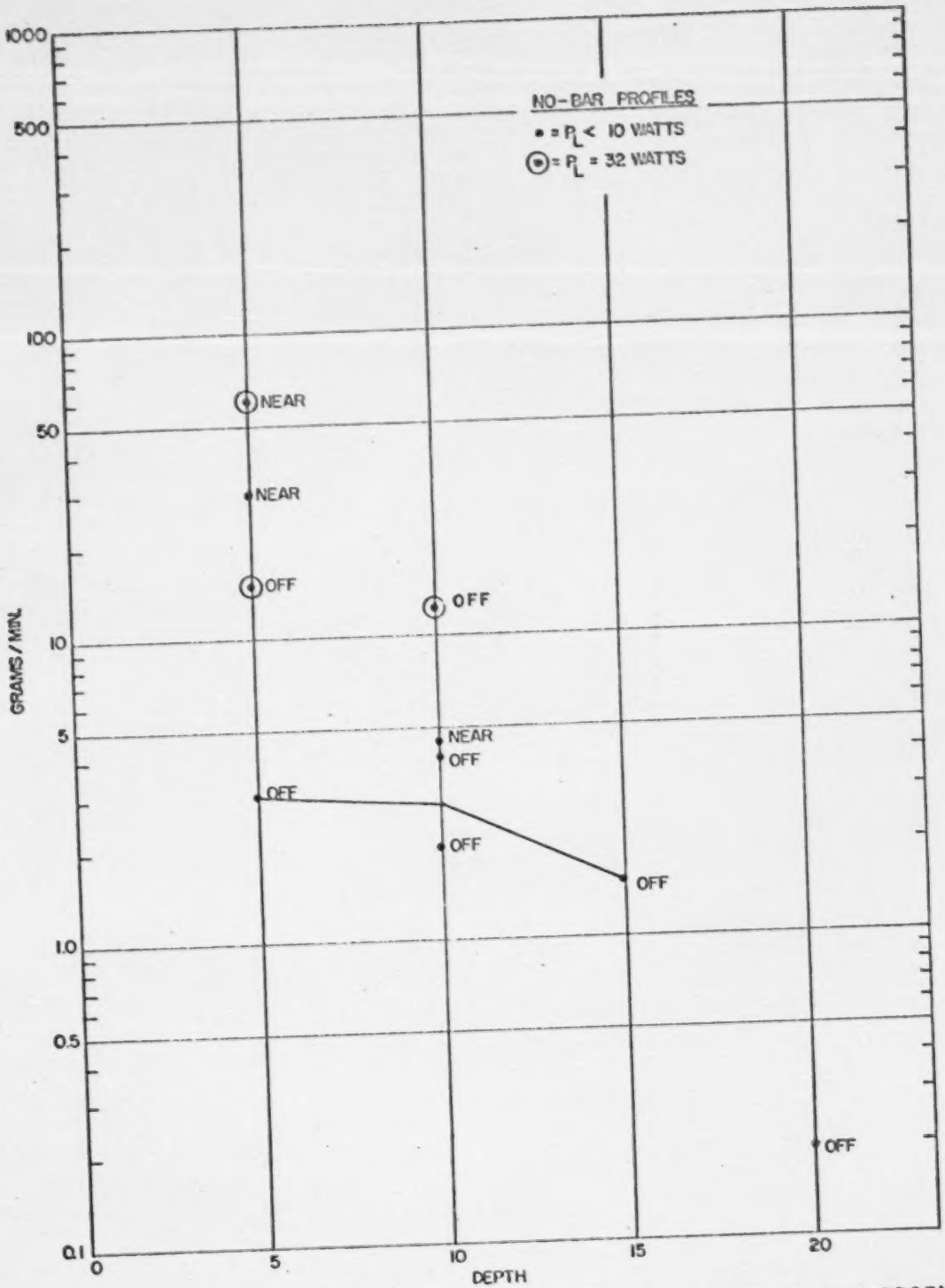

FIGURE 20 QUANTITATIVE RESULTS ON ALL TESTS ON NO-BAR PROFILES

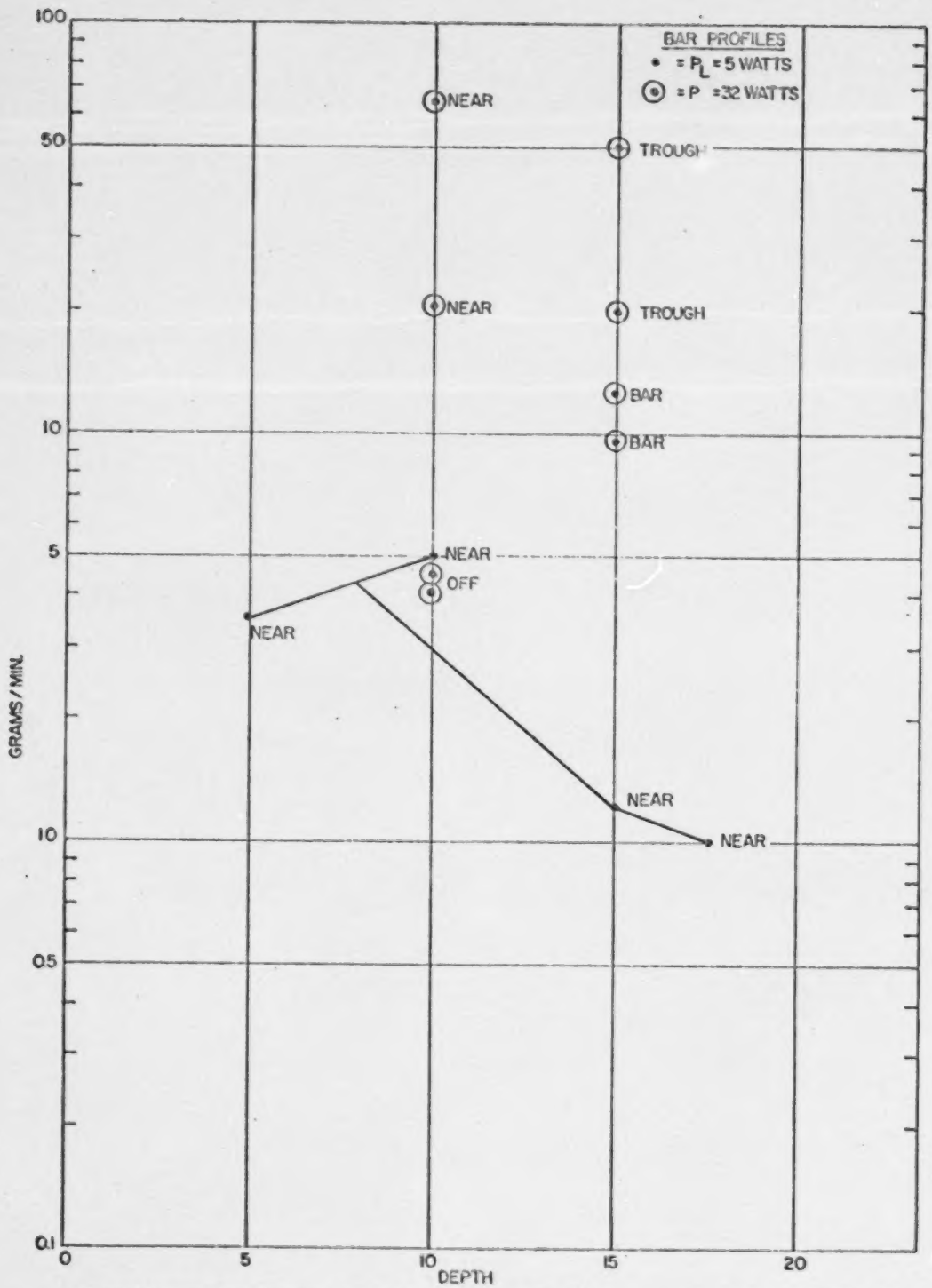

FIGURE 21 QUANTITATIVE RESULTS ON ALL TESTS ON BAR/TROUGH PROFILES

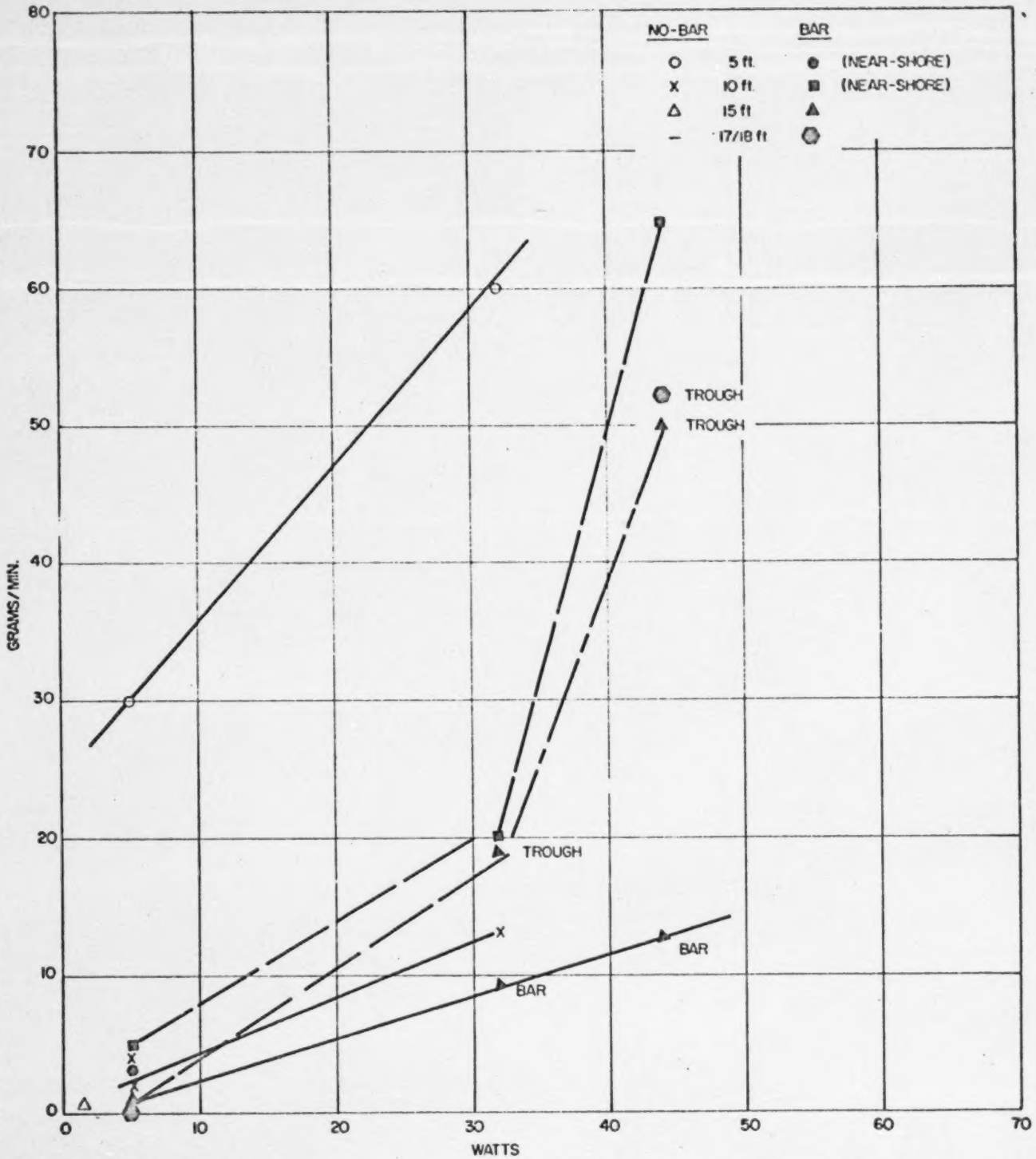

FIGURE 22 LONGSHORE DRIFT AS FUNCTION OF LONGSHORE WAVE ENERGY

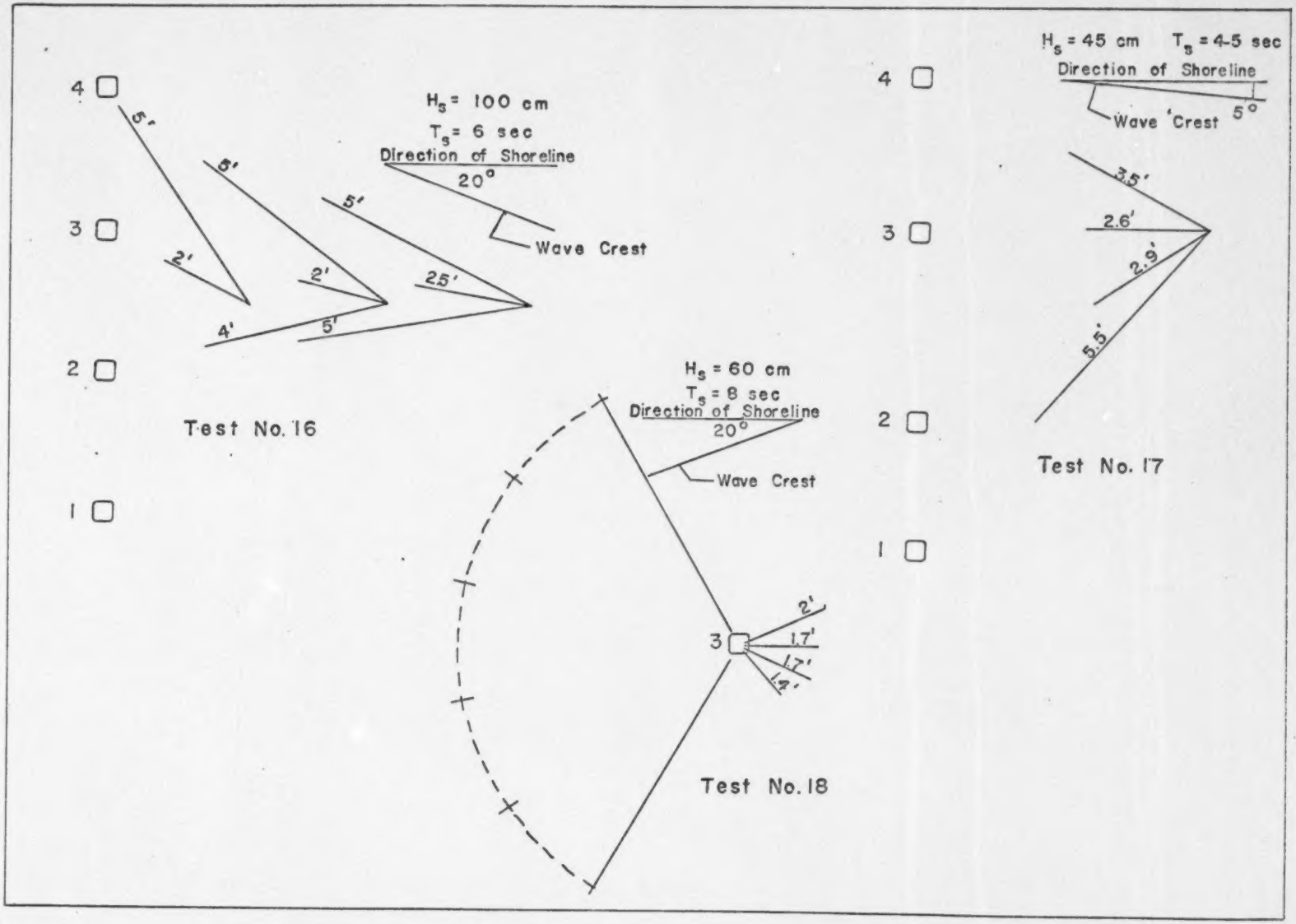

FIGURE 23 MEAN VELOCITIES FOR TRACER GRAINS

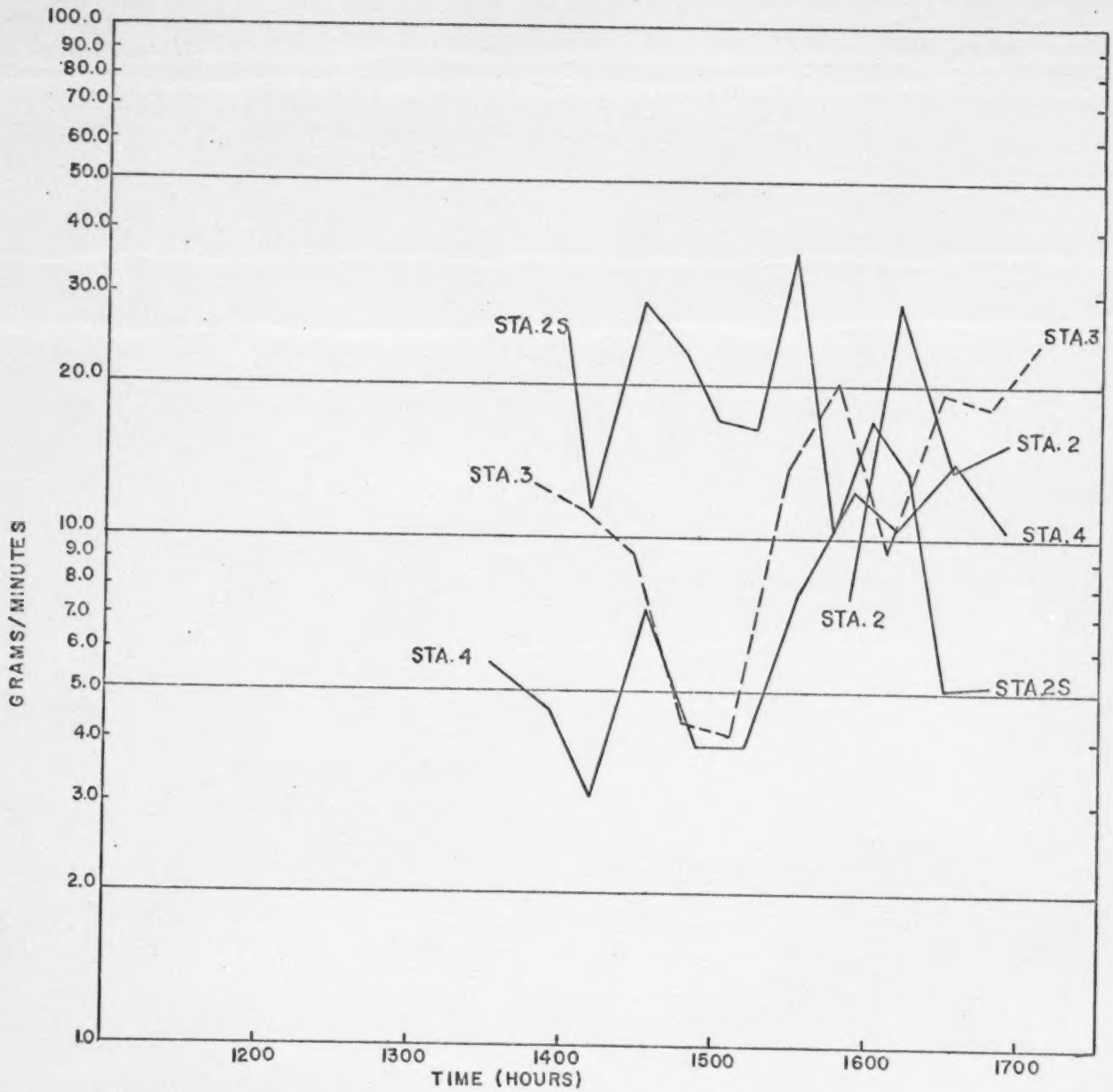

FIGURE 24 QUANTITY OF SEDIMENT MOVING PAST PIER IN FORM OF BEDLOAD AND SUSPENDED LOAD, TEST NO.16 (APRIL 14, 1965)

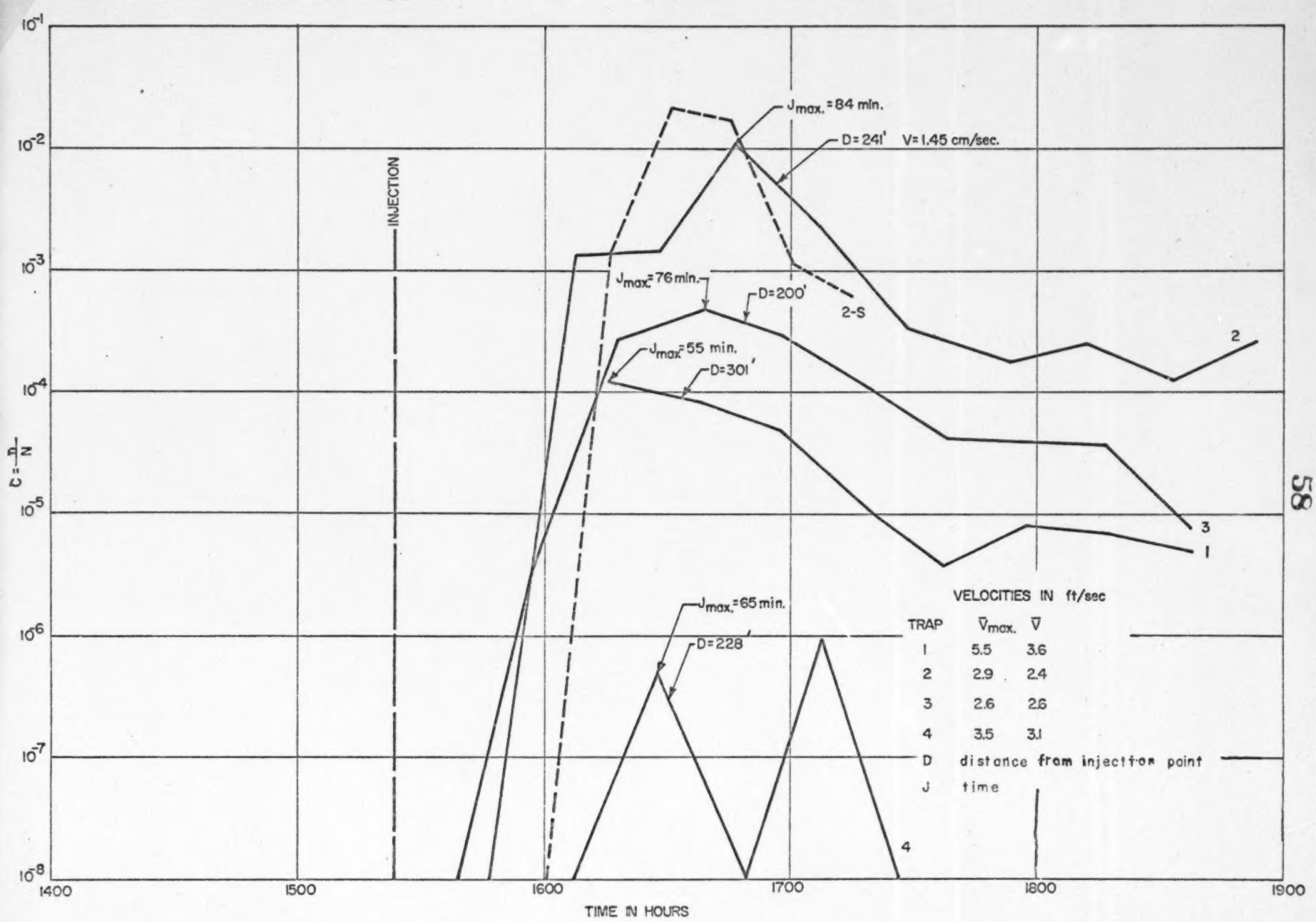

FIGURE 25 DEVELOPMENT OF CONCENTRATIONS AT TEST NO. 17

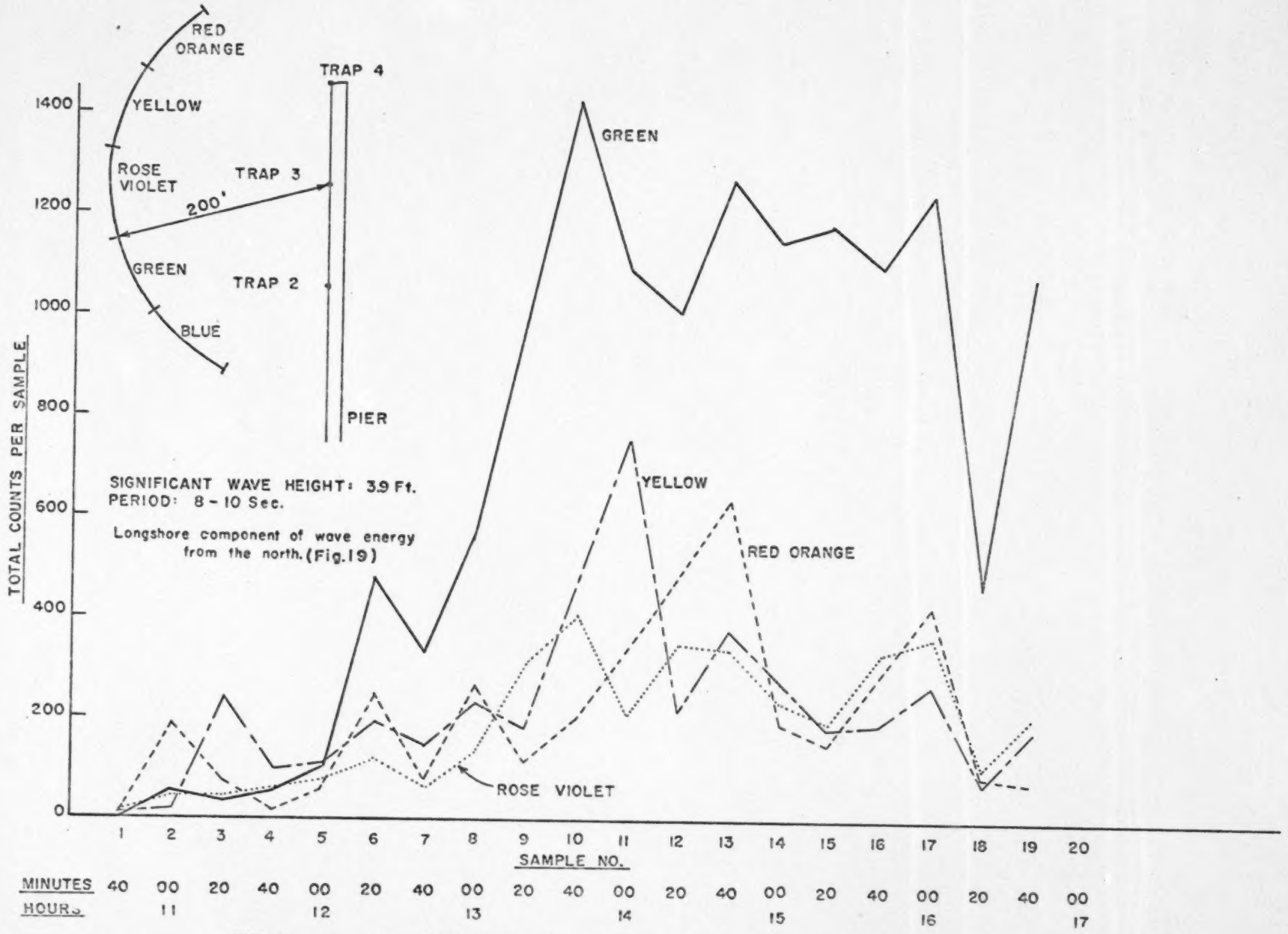

FIGURE 26 DEVELOPMENT OF CONCENTRATIONS AT TEST NO. 18

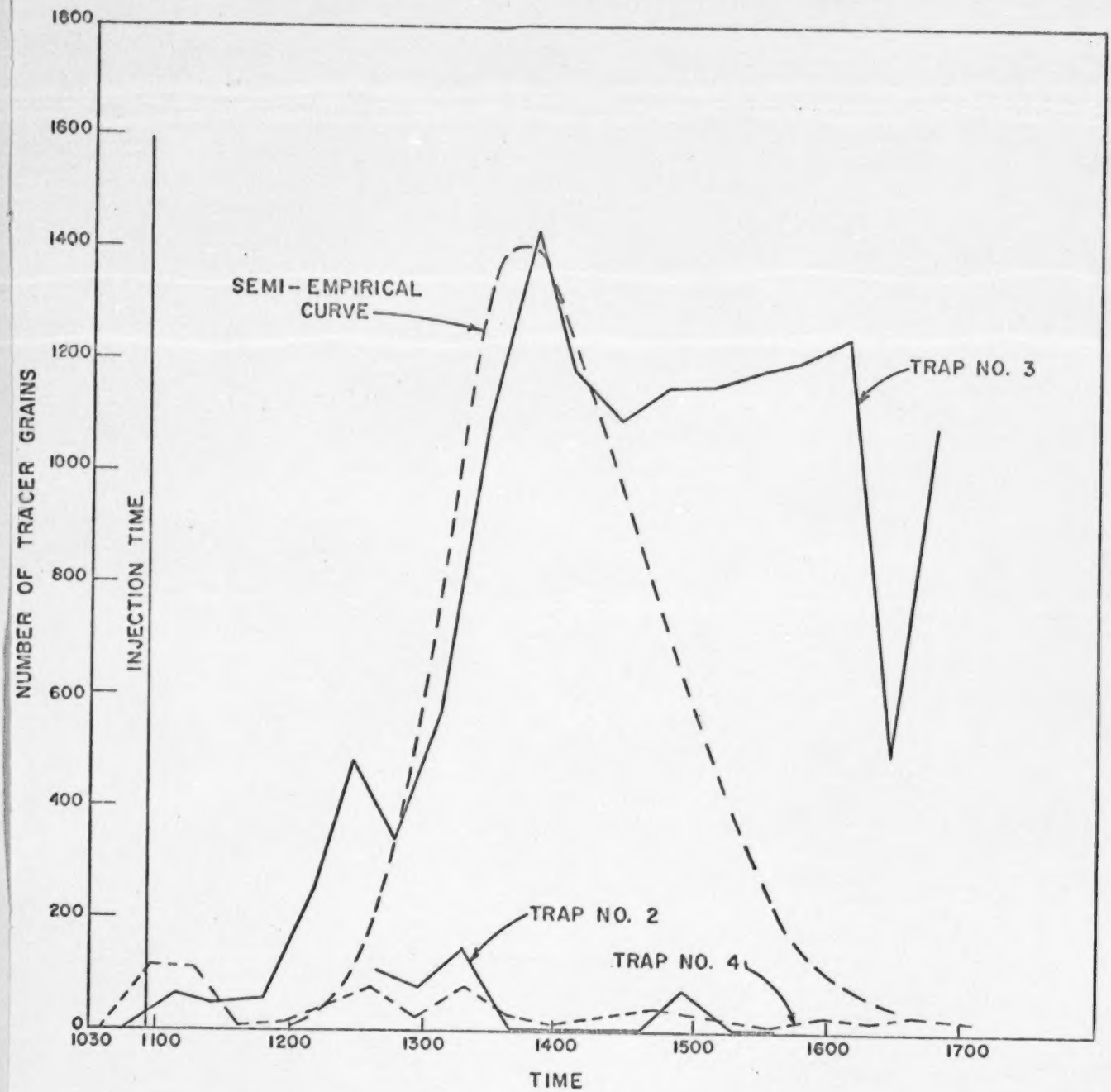

Fig. 27 Comparison of the Semi-empirical Concentration Curve with the Actual Number of Green Tracers in Trap #3, Test No. 18, October 20, 1965.

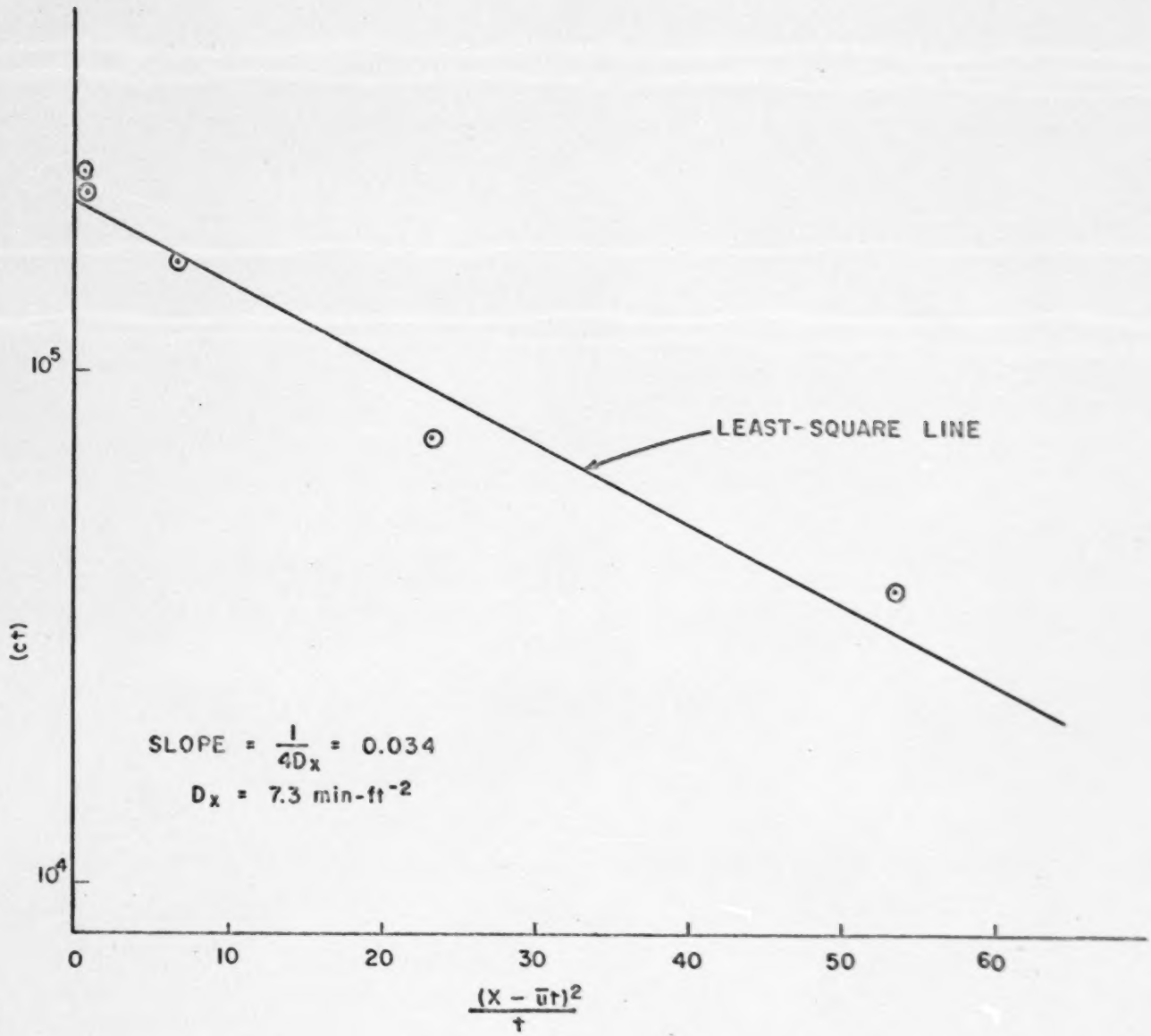

Fig. 28 Determination of Longitudinal Dispersion Coefficient for Green Tracer for Test # 18 20 October 1965

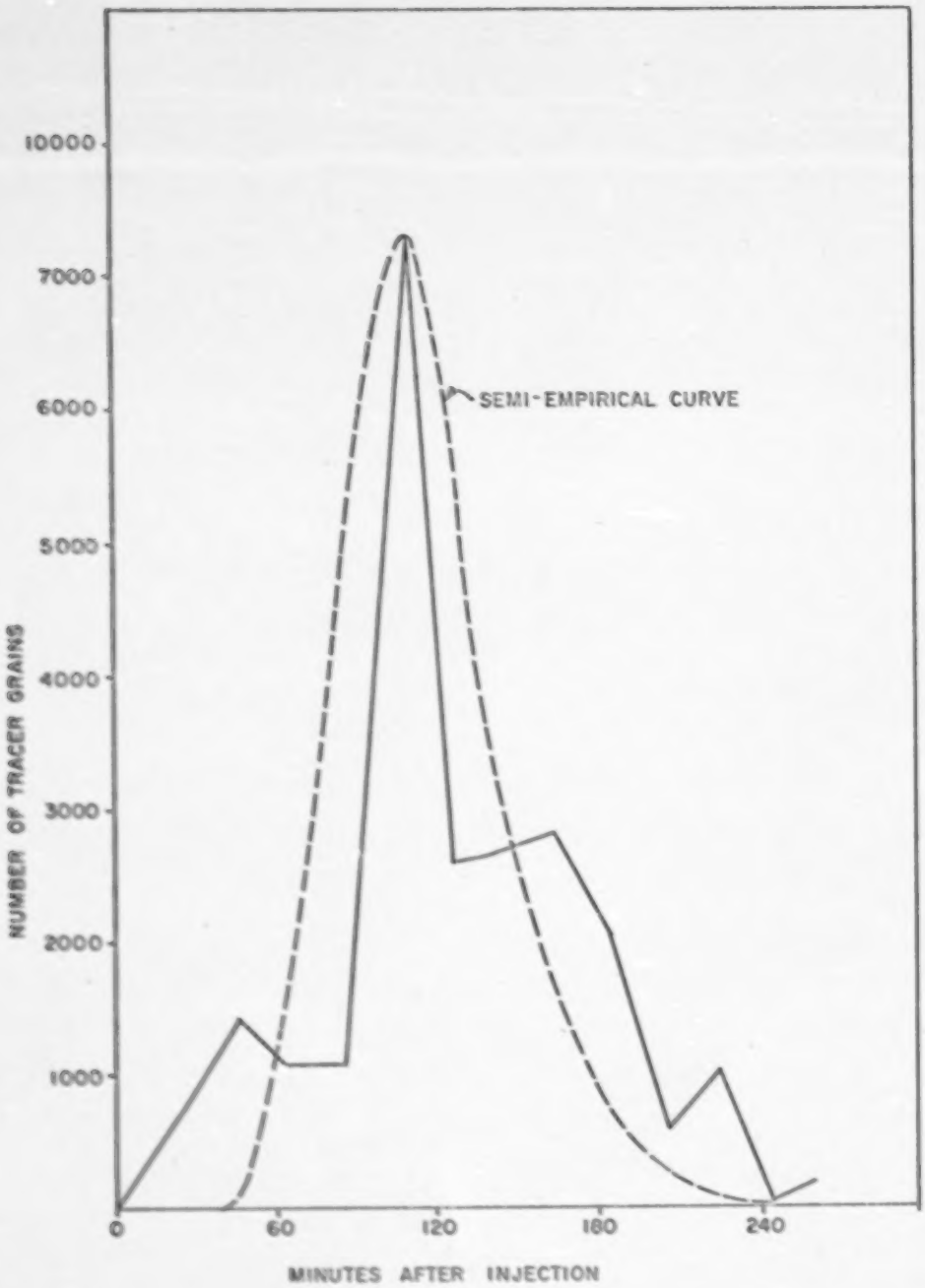

FIGURE 29 COMPARISON OF THE SEMI-EMPIRICAL CONCENTRATION CURVE WITH THE ACTUAL NUMBER OF GREEN TRACERS IN TRAP NO. 5 TEST NO. 19, FEBRUARY 2, 1966

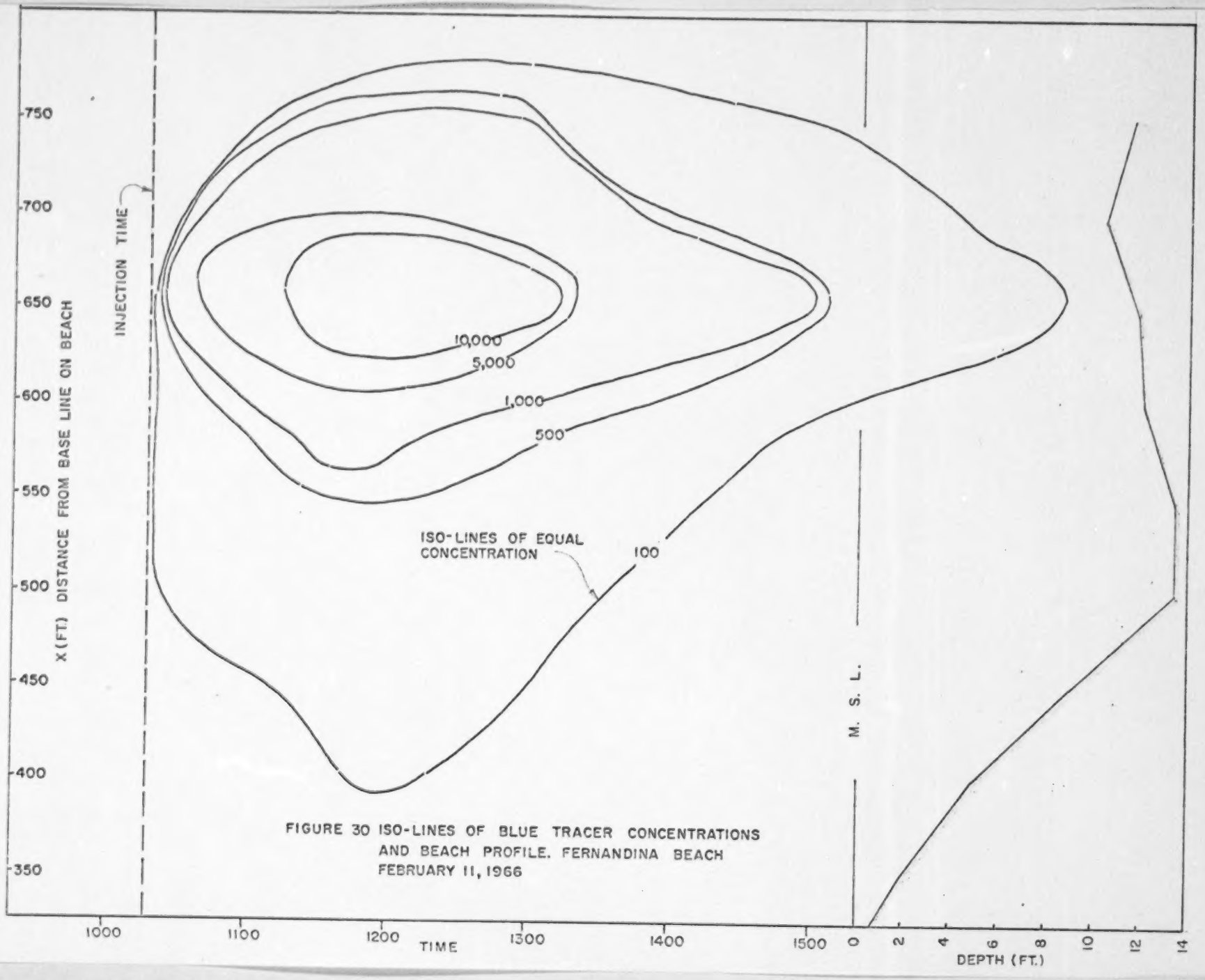

FIGURE 30 ISO-LINES OF BLUE TRACER CONCENTRATIONS AND BEACH PROFILE. FERNANDINA BEACH FEBRUARY 11, 1966